Umbilical mesenchymal stem cells mitigate T-cell compartments shift and Th17/Treg imbalance in acute ischemic stroke via mitochondrial transfer

Shuna Chen[1,2,3†], Chao Han[1,2,4†], Zihan Shi[2,4], Xin Guan[1,2], Liyuan Cheng[1,3], Liang Wang[1,2,4], Wei Zou[2] and Jing Liu[1,2*]

Abstract

Background Acute ischemic stroke (AIS) initiates secondary injuries that worsen neurological damage and hinder recovery. While peripheral immune responses play a key role in stroke outcomes, clinical results from immunotherapy have been suboptimal, with limited focus on T-cell dynamics. Umbilical mesenchymal stem cells (UMSCs) offer therapeutic potential due to their immunomodulatory properties. They can regulate immune responses and reduce neuroinflammation, potentially enhancing recovery by fostering a pro-regenerative peripheral immune environment. However, the effect of UMSCs on T-cell dynamics in AIS remains underexplored. This study investigates T-cell dynamics following AIS and examines how UMSCs may mitigate immune dysregulation to develop better treatment strategies.

Methods AIS patients (NIHSS scores 0–15) were recruited within 72 h of stroke onset, with peripheral blood samples collected on Day 0 (enrollment) and Day 7. T-cell compartments were identified by flow cytometry, and plasma cytokine levels were quantified using a cytometric bead array (CBA). Mitochondria in UMSCs were labeled with MitoTracker. Peripheral blood mononuclear cells from patients were isolated, treated with lipopolysaccharide (LPS), and cocultured with UMSCs in both direct contact and Transwell systems. Flow cytometry, CBA, RT-qPCR, and immunofluorescence assays were used to detect T-cell compartments, gene expression markers for helper T (Th) cell differentiation, cytokine profiles, mitochondrial transfer, reactive oxygen species (ROS) production, and mitochondrial membrane potential. Additionally, mitochondrial DNA in UMSCs was depleted. The effects of UMSCs and mitochondria-depleted UMSCs on ischemic stroke mice were compared through behavioral assessments and analysis of the peripheral immune microenvironment.

Results In AIS, T-cell compartments underwent a phenotypic shift from naïve to effector or memory states, with a specific increase in Th17 cells and a decrease in regulatory T cells, leading to alterations in T-cell-mediated immune functions. In an ex vivo co-culture system, LPS stimulation further amplified these disparities, inducing mitochondrial dysfunction and oxidative stress in T cells. Notably, UMSCs restored mitochondrial function and reversed the shift in T-cell compartments through mitochondrial transfer. Critically, UMSC treatment significantly improved both neurological deficits and peripheral immune disorders in ischemic stroke mice, whereas mitochondria-depleted UMSCs failed to produce this effect.

†Shuna Chen and Chao Han are contributed equally to this work.

*Correspondence:
Jing Liu
liujing@dmu.edu.cn
Full list of author information is available at the end of the article

Chen *et al. Stem Cell Research & Therapy*   (2025) 16:134

Page 2 of 24

Conclusions Our comprehensive insights into the key attributes of T-cell compartments in acute ischemic stroke and the immune regulatory mechanisms of UMSCs provide a crucial theoretical foundation for understanding peripheral immune disorders in ischemic stroke and the therapeutic potential of UMSC treatment.

Keywords Acute ischemic stroke, Umbilical mesenchymal stem cells, Th17/Treg imbalance, T-cell compartment, Mitochondrial transfer

Graphical abstract
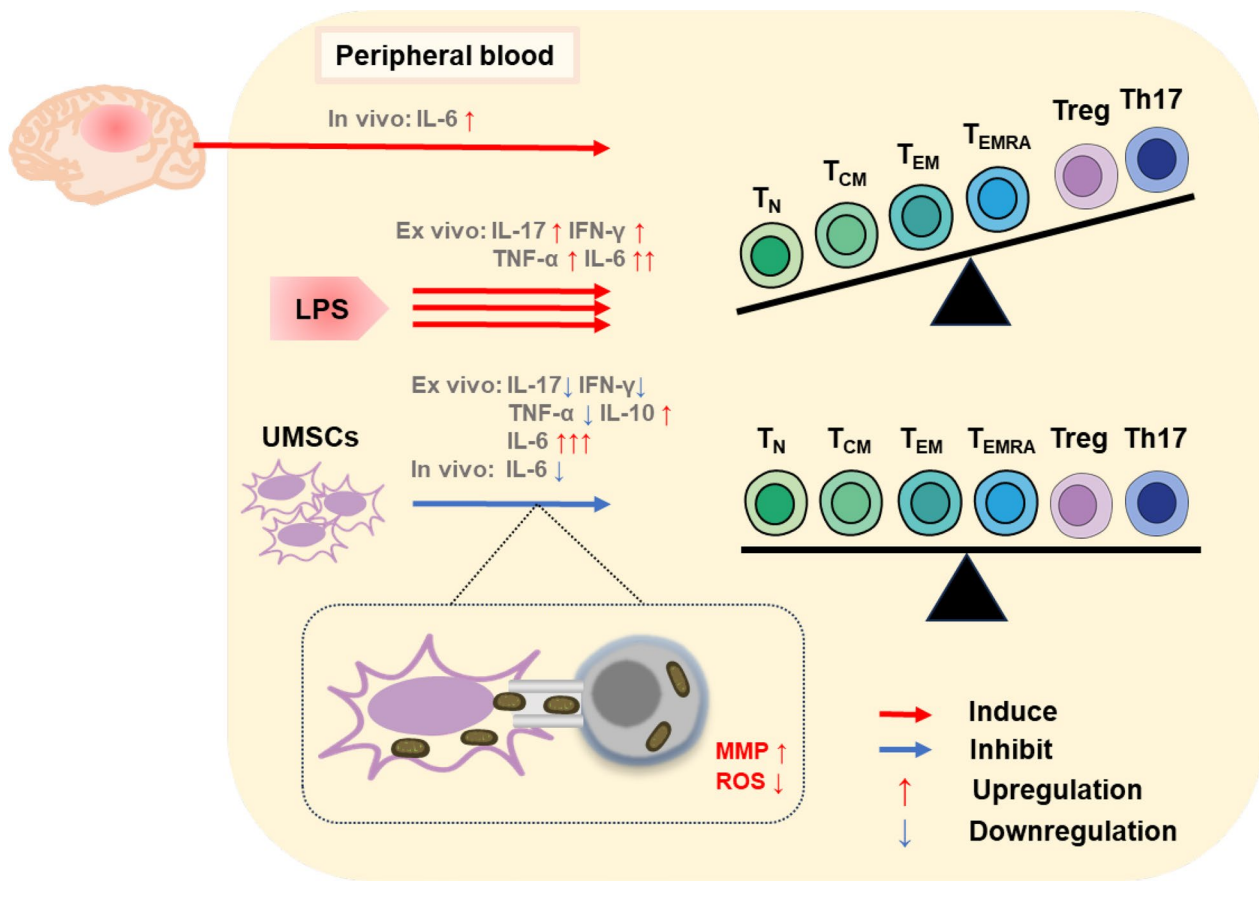
Background

Stroke is the second leading cause of death, with ischemic stroke accounting for 80% of all incidents [1, 2]. Although the primary injury following acute ischemic stroke (AIS) is crucial, time-limited reperfusion therapies and poor neurological outcomes underscore the urgent need for new strategies to address secondary damage [3–5].

Immune responses play a crucial role in the etiology and progression of AIS, sparking increasing interest in their potential as biomarkers and therapeutic targets [6–8]. T cells infiltrate within the first 24 h, peaking at 3–14 days, and persisting up to day 140 [9–11]. In mouse models and AIS patients, brain-infiltrating T cells exhibit activated phenotype, sustaining intracranial inflammation and oxidative stress by secreting pro-inflammatory cytokines [12]. Different T-cell subsets and their cytokines have varying effects on microglia, which in turn influence neuronal survival and tissue regeneration [13]. Recent study shows that T cells can exert effect on microglia even without infiltrating into the parenchyma [14].

However, current clinical trials targeting T cells in AIS, despite success in experimental models, have yielded disappointing results [15]. This may be due to a focus primarily on macroscopic changes in specific effector immune cells, while T cells exhibit remarkable dynamism

Chen *et al. Stem Cell Research & Therapy* (2025) 16:134

Page 3 of 24

and heterogeneity [16]. Recently, the concept of the T cell compartment has emerged, emphasizing the specialization of different T cell subsets and the plasticity of naïve T (T_N) cells throughout their lifecycle [17]. Alongside this, T cell metabolic adaptation has gained increasing attention, with mitochondria and their metabolites playing a central role in T cell survival, differentiation, reprogramming, and effector function [18–20]. The T cell compartment has been shown to significantly modulate self-antigen responses in chronic autoimmune diseases [21–23]. Stroke is no exception, as it activates T_N cells and alters effector T-cell responses [24–27], positioning T-cell dynamics as ideal targets for complementary therapies alongside time-sensitive intravascular treatments.

Stem cell therapy, with its broad therapeutic window, exhibits robust anti-inflammatory effects, holding significant potential for fostering an environment conducive to nerve repair [28]. Umbilical cord mesenchymal stem cells (UMSCs) are particularly valued for their distinct advantages, including broad availability, ease of isolation, low immunogenicity, and minimal ethical concerns [29]. UMSCs can diminish detrimental immune response, thereby protecting against stroke [30–32]. In a study of five stroke patients treated with a single dose of allogenic UMSCs, significant improvements in physiological motor outcomes were observed over a 12-month follow-up period [33]. Although MSCs persist only transiently after intravenous infusion and are quickly cleared, extensive evidence shows that they induce lasting immune regulation [34, 35]. Recent research suggests that direct contact between MSCs and target cells is a crucial mechanism for their function, as MSCs can alleviate mitochondrial dysfunction in recipient cells through mitochondrial transfer [36, 37]. Interestingly, UMSC-mediated mitochondrial transfer plays a significant role in cell reprogramming and immune function across various T-cell subsets [38–42]. However, it remains unclear how UMSCs regulate the peripheral T-cell compartments during stroke and whether mitochondrial trafficking plays a critical role in this process.

In this study, we investigate T-cell dynamics during ischemic stroke and the role of UMSCs. For the first time, we demonstrate that UMSCs restore T-cell compartment balance and mitochondrial function, with mitochondrial transfer playing a pivotal role. This research provides new insights into the role of UMSCs in T-cell-mediated immune mechanisms during stroke recovery.

Methods

Patient enrollment and sample collection

Between October 2022 and November 2023, AIS patients admitted to the First Affiliated Hospital of Dalian Medical University were enrolled within 72 h of symptom onset. Eligible patients were 18–80 years old (inclusive), had a clinical diagnosis of AIS defined by a last known normal score 6–72 h (inclusive) prior to the time of enrollment, and had an NIHSS score of 0–15 points (inclusive) at screening. Patients with scores exceeding 15 were excluded to ensure consistency in the cohort and reduce confounding factors, as severe strokes are often associated with systemic complications and higher variability in immune responses [43–45]. Before stroke, all included patients were able to perform basic activities of daily living without assistance. MRI or CT scans were required for inclusion, with at least one acute infarct in the internal carotid artery system supply area. The vascular risk factor control (VRFC) group included participants with cardiovascular risk factors such as smoking, drinking, hypertension, and diabetes mellitus. Control participants were matched for age, sex, and vascular risk factors, and had no history of cerebrovascular disease. Exclusion criteria included ongoing therapy for infectious diseases, clinical or subclinical signs of infection, or the use of immunomodulatory drugs. The study was approved by the Ethics Review Committee of the Stem Cell Clinical Research Institution of the First Affiliated Hospital of Dalian Medical University (No. YJ-GXB-2022-01, Dalian, China), and written informed consent was obtained from all patients or their surrogates. EDTA-anticoagulated blood was drawn within 72 h of stroke onset (baseline) and again 7 days after stroke. Blood from VRFC participants was collected only on the day of enrollment. Sample size calculations indicated that a minimum of 58 participants (19 controls and 39 AIS patients) would be required to achieve 80% power and an α level of ≤ 0.05 (GPower software, version 3.1). The final study included 20 participants in the control group and 62 participants in the AIS group, thus meeting the statistical requirements.

PBMC-UMSC ex vivo coculture system

Six patients with AIS were selected (see Table S1 for patient information), and fasting venous blood was collected within 72 h of onset. Human UMSCs were prepared at the Stem Cell Clinical Research Center of the First Affiliated Hospital of Dalian Medical University, as previously described [46]. The cell quality was reviewed and certified by the China National Medical Products Administration. Before use, the biological characteristics of UMSCs were further verified (Fig. S1) and confirmed to meet the criteria for MSCs as defined by the International Society for Cell and Gene Therapy [47]. UMSCs were seeded at 5×10^5 cells per well in regular 6-well plates overnight at 37 °C. Peripheral blood mononuclear cells (PBMCs) were isolated within 60 min of venipuncture by density gradient centrifugation at $300 \times g$ for 30

min using Ficoll-Paque PLUS (GE Healthcare, Sweden). The collected PBMCs were either directly seeded onto UMSCs (5×10^5 cells per well) in a direct contact coculture system (CC system) or seeded into a Transwell chamber (0.4 μm, Corning, USA) placed above UMSCs in an indirect contact coculture system (TW system). The cells were incubated in X-VIVO™ 15 medium (Lonza, Switzerland) supplemented with 10% fetal bovine serum (FBS, OriCell, China) and IL-2 (1×10^2 U/mL, Proleukin, USA) (Fig. 3A shows the experimental design). Lipopolysaccharide (LPS) from Escherichia coli O111:B4 (Sigma Aldrich, USA) was added to the culture medium at a concentration of 100 ng/mL, as previously described [48, 49]. The culture was maintained at 37°C with saturated humidity and 5% CO_2 . After 72 h of coculture, both PBMCs and the supernatant were collected for further analysis.

Flow cytometry

For the identification of the patient's T-cell phenotype, whole blood was stained at room temperature for 30 min with various cocktails of fluorochrome-conjugated antibodies (Table S2). Red blood cells were lysed by adding lysing solution (BD Pharm Lyse, USA) according to the manufacturer's instructions. For the identification of cocultured PBMCs, cells were collected, washed twice with phosphate-buffered saline (PBS), resuspended in staining buffer (BD Pharmingen, USA), and incubated with the antibodies. For the identification of mice immune cell phenotype, T cells were isolated from whole blood using an isolation solution (TBD Science, China) and then stained with fluorochrome-conjugated antibodies (Table S3) following the manufacturer's instructions (BD Biosciences, USA). Immunophenotyping panels were adapted from previous publications [50, 51]. Samples were analyzed using a flow cytometer (SH800S, Sony, Japan), and data were processed using FlowJo software (Treestar, Inc., Ashland, OR, USA). T cells were identified based on the following panels:

Human panel:

T-cell subsets: T cells, $CD45^+CD3^+$; helper T lymphocytes (Th cells), $CD45^+CD3^+CD4^+$; and cytotoxic T lymphocytes (Tc cells), $CD45^+CD3^+CD8^+$; among Th cells, we identified: Th1 cells, $CXCR3^+CCR6^-$; Th2 cells, $CXCR3^-CCR6^-$; Th17 cells, $CXCR3^-CCR6^+$; and regulatory T (Treg) cells, $CD25^+CD127^{low}$.

T-cell compartments: naïve T (T_N) cells, $CD3^+CD45RA^+CCR7^+$; central memory T (T_{CM}) cells, $CD3^+CD45RA^-CCR7^+$; effector memory T (T_{EM}) cells, $CD3^+CD45RA^-CCR7^-$; terminally differentiated effector memory T (T_{EMRA}) cells, $CD3^+CD45RA^+CCR7^-$.

Mouse panel:

T-cell subsets: T cells: $CD45^+CD3^+$; Th cells: $CD45^+CD3^+CD4^+$; Tc cells: $CD45^+CD3^+CD8^+$; Th17 cells: $CD3^+CD4^+ROR\gamma t^+$; Treg cells: $CD3^+CD4^+CD25^+FOXP3^+$.

T-cell compartments: T_N cells, $CD3^+CD44^-CD62L^+$; T_{CM} cells, $CD3^+CD44^+CD62L^+$; T_{EM} cells, $CD3^+CD44^+CD62L^-$; exhausted T cell (T_{EX} cells), $CD3^+PD-1^{high}$.

Cytometric bead array (CBA) assay

For plasma collection, whole blood was centrifuged (3000 rpm, 4 °C, 15 min), and the samples were stored immediately at -80 °C. The quantitative detection of cytokines was performed via a CBA assay. The concentrations of IL-2, IL-4, IL-6, IL-10, IL-17A, TNF-α, and IFN-γ were measured with a Human LEGENDplex™ Kit (BioLegend, USA) or Mouse Th1/Th2/Th17 Cytokine Kit (BD Biosciences) following the manufacturer's instructions. Cytokine levels were analyzed using a flow cytometer (SH800S).

Mitochondrial transfer assessment

To examine mitochondrial transfer, UMSCs were labeled with 1 μM MitoTracker® Deep Red FM (Invitrogen, USA) according to the manufacturer's instructions. After a 30-min incubation at 37°C, the cells were washed twice, and LPS-induced PBMCs were seeded onto UMSCs in either the CC or TW coculture system, as described above. Based on previous studies showing 72 h as the optimal time point for organelle transfer analysis [42], this time point was used in our experiments. After 72 h, the efficiency of mitochondrial transfer from UMSCs to PBMCs was assessed using confocal laser scanning microscopy (Yokogawa, Japan) and flow cytometry (SH800S).

Reactive oxygen species (ROS) and mitochondrial membrane potential (MMP) measurement

Mitochondrial function in PBMCs was monitored by assessing the MMP and ROS levels using a JC-1 assay (JC-1 MitoMP Detection Kit, Dojindo, Japan) and a ROS assay (ROS Assay Kit-Highly Sensitive DCFH-DA, Dojindo). Briefly, after 72 h of coculture with UMSCs under LPS stimulation, PBMCs were collected and incubated with 2 μM 2′, 7′-dichlorofluorescein diacetate (DCFH-DA) or JC-1 working solution at 37 °C according to the manufacturer's instructions. Finally, JC-1 and ROS probe fluorescence was analyzed using flow cytometry (SH800S) and confocal laser scanning microscopy (Yokogawa).

Reverse transcription-quantitative PCR (RT-qPCR)

The experiment was performed according to the manufacturer's instructions. Briefly, PBMCs were collected from the coculture system, and total RNA was extracted (Accurate Biology, China). Complementary DNA (cDNA) was then synthesized (Accurate Biology). RT-qPCR was conducted using SYBR Green Pro Taq HS (Accurate Biology) and specific primers for Th cell subset marker genes: T-bet (for Th1), GATA3 (for Th2), RORγt (for Th17), and FOXP3 (for Treg), as listed in Table S4. RT-qPCR was performed on a BioRad CFX Thermal Cycler using the following protocol: 1) 95℃ for 30 min, 2) 95℃ for 2 min, and 3) 40 cycles at 95℃ for 5 s and 60℃ for 30 s. Relative gene expression levels were calculated using the ΔΔCT method, with GAPDH serving as the internal control.

Mitochondrial DNA (mtDNA) depletion and RT-qPCR verification

A 1000× stock of 2′,3′-dideoxycytidine (ddC, Sigma, Cat. # D5782) was prepared in water and added to UMSCs cultured in complete media to achieve a final concentration of 3 μg/mL, as previously described [52]. Cells were passaged every 1–3 days, with fresh ddC added each time. Following ddC treatment, RT-qPCR was performed to quantify mtDNA-encoded MT-ND1, normalized to nucleus-encoded B2M using primers listed in Table S4. Samples were compared by calculating ΔΔCT and fold differences.

Cerebral ischemia model and UMSC in vivo administration

All experimental studies were approved by the Ethics Committee of the Animal Experiment Center of Dalian Medical University and conducted following the Guide for the Care and Use of Laboratory Animals of the National Institutes of Health (Ethical No. AEE23127, Feb. 28, 2023). Healthy male C57BL/6J mice (8−10 weeks old, weighing 25–30 g) were purchased from the Animal Experiment Center of Dalian Medical University. The mice were housed and bred under specific pathogen-free conditions in a temperature-controlled environment with a 12-h light/dark cycle at the animal central laboratory. Mice were randomly assigned to one of the following groups: Sham, MCAO, MCAO+UMSCs, or MCAO+UMSCs (ddC) (n=5 mice/group) based on a computer-generated block randomization list. Focal cerebral ischemic stroke models were established as previously described [53]. Briefly, anesthesia was induced with 2% isoflurane (RWD Life Science, China) and maintained during surgery with 1.5% isoflurane in regular air. Focal cerebral ischemia was induced by inserting a monofilament through the external carotid artery (ECA) and internal carotid artery (ICA) to occlude the middle cerebral artery (MCA) for 45 min, followed by removal of the filament to allow reperfusion. Sham surgery was performed similarly, except without occlusion. After 2 h of reperfusion, mice in the UMSC treatment group received a tail vein injection of 100 μL containing $6×10^6$ UMSCs or mitochondria-depleted UMSCs (ddC). Mice in the Sham and MCAO groups received the same volume of saline via tail vein injection. Temporal muscle temperature was maintained at 37℃±0.5℃ during surgery and for up to 3 h post-surgery. This experiment was conducted as a double-blind study during both behavioral and experimental tests to minimize potential subjective biases. No adverse events occurred, and no animals or units were excluded.

5-Triphenyl tetrazolium chloride (TTC) staining

Three days after the onset of MCAO, the mice were deeply anesthetized using 10% isoflurane in an induction chamber (as recommended by the AVMA Guidelines for the Euthanasia of Animals: 2020 Edition [54]) until complete loss of righting reflex and response to toe pinch was observed. Following deep anesthesia, euthanasia was confirmed by cervical dislocation. The brains were removed from the skull and sliced into 2 mm coronal sections. The slices were incubated in 2% TTC (Solarbio, China) solution at 37℃ for 15 min, then stored in 4% paraformaldehyde (Solarbio) for 24 h for later visualization. The infarcted and ipsilateral hemisphere areas were measured using ImageJ software (version 1.8.0, National Institutes of Health, USA).

Mouse behavioral analysis

Longa test: The Longa test was scored on a five-point scale: a score of 0 indicated no neurologic deficit, a score of 1 (failure to extend left forepaw fully) a mild focal neurologic deficit, a score of 2 (circling to the left) a moderate focal neurologic deficit, and a score of 3 (falling to the left) a severe focal deficit; rats with a score of 4 did not walk spontaneously and had a depressed level of consciousness [55].

Cylinder test: The cylinder test was conducted as previously described [56] to monitor the severity and recovery of sensorimotor deficits after focal cerebral ischemia in mice. Briefly, mice were allowed to acclimate to the testing environment for 30 min under stable conditions (appropriate temperature and humidity) in a quiet laboratory setting. Each mouse was then gently held by the tail and placed into a transparent glass cylinder with a radius of 10 cm and a height of 30 cm. The number of times the contralateral forelimb touched the cylinder wall was monitored and recorded over a 5-min period. Each mouse underwent the test three times. Data were collected, and the percentage of touches on the

Chen *et al. Stem Cell Research & Therapy*   (2025) 16:134

Page 6 of 24

impaired side was calculated using the formula: (number of impaired side touches/total number of touches)×100.

Statistical analysis

Comparisons of clinical data were performed using a generalized linear model. Continuous variables are presented as the mean±standard deviation (SD) for normally distributed data, or as the median with interquartile ranges (IQR) for non-normally distributed data. For continuous data, either a t-test or Mann–Whitney U test was used for two-group comparisons, and one-way ANOVA with the LSD post hoc test or Welch's t-test with Dunnett's post hoc test was used for multiple-group comparisons, as appropriate. Correlation analysis was performed using Spearman's rank correlation test. All statistical analyses were conducted using SPSS software version 20.0 (SPSS Inc., Chicago, IL, USA) and GraphPad Prism 9 (GraphPad Software, San Diego, CA, USA). A *p*-value of <0.05 was considered statistically significant; ns indicates not significant or $p \geq 0.05$, $*p < 0.05$, $**p < 0.01$, and $***p < 0.001$.

Results

Baseline characteristics of the patient cohort

The stroke group consisted of 42 men and 20 women, with an average age of 67.02 years (range, 45–80 years). The control group included 10 men and 10 women, with an average age of 64.65 years (range, 50–77 years). According to imaging results at enrollment, the infarction locations in stroke patients were all within the supply area of the ICA system. Differences in demographic variables and clinical data between the two groups are summarized in Table 1. Generalized linear model analysis of all indicators revealed no statistically significant differences in baseline data between the two groups ($p > 0.05$).

T cells undergo phenotype changes leading to Th17/Treg imbalance following stroke.

To characterize T-cell heterogeneity, we gated T cells to identify Th and Tc cells, as well as Th1, Th2, Th17, and Treg subsets within the Th cell population using established markers (Fig. 1A, Table S2), and performed correlation analysis with stroke severity (NIHSS score). The statistical data are presented in Table S5. Quantification of the manually gated populations revealed a modest decrease in T and Th cell populations, along with an increase in Tc cell population in AIS patients (Fig. S2A); however, after adjusting for baseline clinical data, including age, sex, and comorbidities, the difference was not statistically significant ($p > 0.05$). Moreover, a negative correlation was observed between Tc-cell frequency and NIHSS score at the time of

Table 1 Demographic and clinical characteristics of VRFC and AIS patients

	VRFCs (N=20)	AIS patients (N=62)	*p*-value
Age, years, mean (SD)	64.65 (8.59)	67.02 (7.72)	0.175
Gender, male, n/N (%)	10/20 (50%)	42/62 (67.7%)	0.182
Smoker, n/N (%)	7/20 (35%)	33/62 (53.2%)	0.389
Drinker, n/N (%)	3/20 (15%)	19/62 (30.6%)	0.931
Hypertension, n/N (%)	12/20 (60%)	46/62 (74.2%)	0.691
Diabetes mellitus, n/N (%)	9/20 (45%)	26/62 (41.9%)	0.581
Stroke severity (NIHSS)			
Mild (0–4), n/N (%)	–	21/62 (33.9%)	–
Moderate (5–15), n/N (%)	–	41/62 (66.1%)	–
Triglyceride, medium (IQR)	1.33 (0.96–1.7)	1.45 (0.97–2.09)	0.262
Total cholesterol, mean (SD)	4.57 (1.54)	4.91 (1.23)	0.524
HDL-C, mean (SD)	1.25 (0.33)	1.16 (0.25)	0.906
LDL-C, mean (SD)	2.5 (1.12)	2.79 (0.8)	0.430
WBC, mean (SD)	6.18 (0.93)	6.69 (1.42)	0.244
Neutrophils, mean (SD)	3.93 (0.83)	4.32 (1.16)	0.274
Lymphocytes, medium (IQR)	1.78 (1.36–2.2)	1.73 (1.3–2.41)	0.273
Monocytes, medium (IQR)	0.37 (0.29–0.43)	0.34 (0.27–0.44)	0.407

Measurement data are expressed as the mean (SD) or median (IQR). Enumeration data are presented as n/N (%), where n represents the actual number, N represents the total number of observations with available data, and % represents the percentage of n relative to N. *p* values represent comparisons between groups via a generalized linear model. All indicators in the table were included in the model during analysis

VRFC vascular risk factor control, *AIS* acute ischemic stroke, *SD* standard deviation, *IQR* interquartile range, *NIHSS* National Institutes of Health Stroke Scale, *WBC* white blood cell, *HDL-C* high-density lipoprotein cholesterol, *LDL-C* low-density lipoprotein cholesterol

enrollment ($r = 0.288$, $p = 0.023$; Fig. S2D). As shown in Fig. 1B, the frequencies of Th1 and Th2 populations remained unchanged ($p > 0.05$), whereas Th17 cells significantly increased within 3 days of stroke onset ($p = 0.020$), which was positively correlated with stroke severity ($r = 0.368$, $p = 0.020$; Fig. 1C), and returned to baseline levels by day 7 ($p = 0.507$). The Treg cell population gradually decreased over time and was significantly lower 7 days after stroke onset compared to day 3 ($p = 0.029$; Fig. 1B). However, after adjusting for confounding factors, the difference between the Treg levels in AIS patients and controls was not statistically significant ($p = 0.140$). Given the instability and plasticity of Th17 cells, which can undergo global genetic reprogramming and differentiate into Treg cells [57], we

Chen *et al. Stem Cell Research & Therapy*   (2025) 16:134

Page 7 of 24

considered the Th17/Treg ratio as a combined measure to investigate their role during acute stroke. Compared to the control group, the Th17/Treg ratio was significantly elevated within 3 days of stroke onset ($p = 0.001$) and remained elevated through 7 days, even after adjustment for confounding factors ($p = 0.001$; Fig. 1D). This ratio was positively correlated with stroke severity ($r = 0.388$, $p = 0.002$; Fig. 1D).

T-cell cytokine production is essential for T-cell function and intercellular communication [58]. To investigate stroke-induced changes in cellular immune function, we quantified inflammatory cytokines in the peripheral blood of AIS patients (statistical data are shown in Table S6). The concentrations of IL-2, IL-4, IL-6, IL-10, IL-17, IFN-γ, and TNF-α from both the control group and AIS patients within 3 days of stroke onset were analyzed using a generalized linear model (Fig. S3). Among these, only the IL-6 concentration was significantly elevated in AIS patients ($p = 0.047$; Fig. 1F), even after accounting for confounding factors ($p = 0.019$), and was positively correlated with stroke severity ($r = 0.829$, $p < 0.001$; Fig. 1G). IL-6 levels remained significantly higher at 7 days post-stroke onset compared to control patients ($p = 0.008$), and were further elevated compared to the acute phase of stroke ($p < 0.001$). IL-10, which plays a crucial role in limiting inflammation and maintaining immune homeostasis by promoting the development of Treg cells [59], did not show significant changes during AIS ($p > 0.05$; Figure S3C).

The polarization of Th cell populations, particularly the increase in proinflammatory Th17 cells and a reduction in Tregs, has been linked to impaired immune responses following stroke and increased susceptibility to infections [60]. Moreover, stroke-induced systemic immunosuppression further compromises the immune response, exacerbating the risk of infections [61]. Studies have shown that stroke patients, particularly those who develop infections, exhibit a significant decrease in CD4$^+$ Th cell counts alongside elevated plasma IL-6 levels [62]. Overall, our findings suggest that an increased Th17/Treg ratio and sustained IL-6 elevation may serve as valuable indicators for immune monitoring and potential biomarkers of stroke severity during both the acute and subacute phases.

The post-stroke shift of naïve T cells to effector and memory states is correlated with clinical severity.

To investigate the dynamic characteristics of T-cell differentiation following stroke, we characterized the T-cell compartment based on CD45RA and CCR7 expression on CD4$^+$ and CD8$^+$ T cells (Table S2). As shown in Fig. 2A, we identified T_{EMRA}, T_N, T_{CM}, and T_{EM} in the enrolled patients using well-established markers (statistical data are shown in Table S5) [50]. We found that both CD4$^+$ and CD8$^+$ T-cell compartments shift from the naïve population to memory or terminally differentiated effector populations. Specifically, as shown in Fig. 2B, within the CD4$^+$ T-cell population, AIS patients exhibited a significant decrease in the proportion of T_N cells within 3 days of stroke onset compared to control patients ($p = 0.023$). Conversely, the proportion of T_{EMRA} cells increased significantly ($p = 0.007$), and this increase persisted into the subacute phase of ischemic stroke ($p = 0.004$). Within the CD8$^+$ T-cell population, as shown in Fig. 2E, T_N cells also showed a significant decrease within 3 days after stroke ($p = 0.020$), while the T_{EM} cell population remained elevated during the acute ($p = 0.006$) and subacute ($p = 0.046$) phase of stroke. Additionally, the frequencies of CD4$^+$ ($r = -0.666$, $p < 0.001$; Fig. 2C) and CD8$^+$ ($r = -0.346$, $p = 0.006$; Fig. 2F) T_N cells were negatively correlated with stroke severity. Although the CD4$^+$ T_{EM} cell population showed no significant change during stroke, its frequency was positively correlated with stroke severity ($r = 0.332$, $p = 0.011$; Fig. 2D). Research indicates that the differentiation of T_N cells follows a linear lineage

(See figure on next page.)

Fig. 1 Longitudinal analysis of T-cell subsets and cytokine concentrations in the peripheral blood of patients post-stroke. **A** Representative FACS plots showing the flow cytometric gating strategy used to identify T (CD3$^+$), Th (CD3$^+$CD4$^+$) and Tc (CD3$^+$CD8$^+$) cells within the PBMC population, as well as Th1 (CXCR3$^+$CCR6$^-$), Th2 (CXCR3$^-$CCR6$^-$), Th17 (CXCR3$^-$CCR6$^+$) and Treg (CD25$^+$CD127^{low}) cells within the Th cell population. **B** Frequency and distribution of Th cell subsets among CD4$^+$ T cells in VRFC and AIS patients. Data are represented as percentages of total CD4$^+$ T cells. The pie chart shows the mean relative proportions of different Th cell subsets within the CD4$^+$ T cell population in VRFC and AIS patients. **C** Correlation plots of the baseline Th17 cell percentage with NIHSS score. **D** Th17/Treg ratio in VRFC and AIS patients and its correlation with NIHSS score (**E**). **F** IL-6 concentrations in VRFC and AIS patients. **G** Correlation plots of the baseline IL-6 concentration with NIHSS score. Data in **B** and **D** are presented as scatter plots showing mean with SD, while data in **F** are presented as scatter plots showing median with IQR. For correlations, the regression line and standard error are shown. Statistical comparisons between AIS and VRFC patients were performed via generalized linear models, adjusting for age, sex, smoking, drinking, hypertension, and diabetes mellitus. Statistical comparisons between baseline and 7-day data among AIS patients were made using the Mann–Whitney U test. Correlation analysis was conducted with Spearman's rank correlation test. *p* values < 0.05 are considered statistically significant. ns indicates not significant or $p \geq 0.05$; *$p < 0.05$, **$p < 0.01$, and ***$p < 0.001$. Abbreviations: PBMC, peripheral blood mononuclear cell; Th cell, helper T cell; Tc cell, cytotoxic T cell; Treg cell, regulatory T cell; IL, interleukin
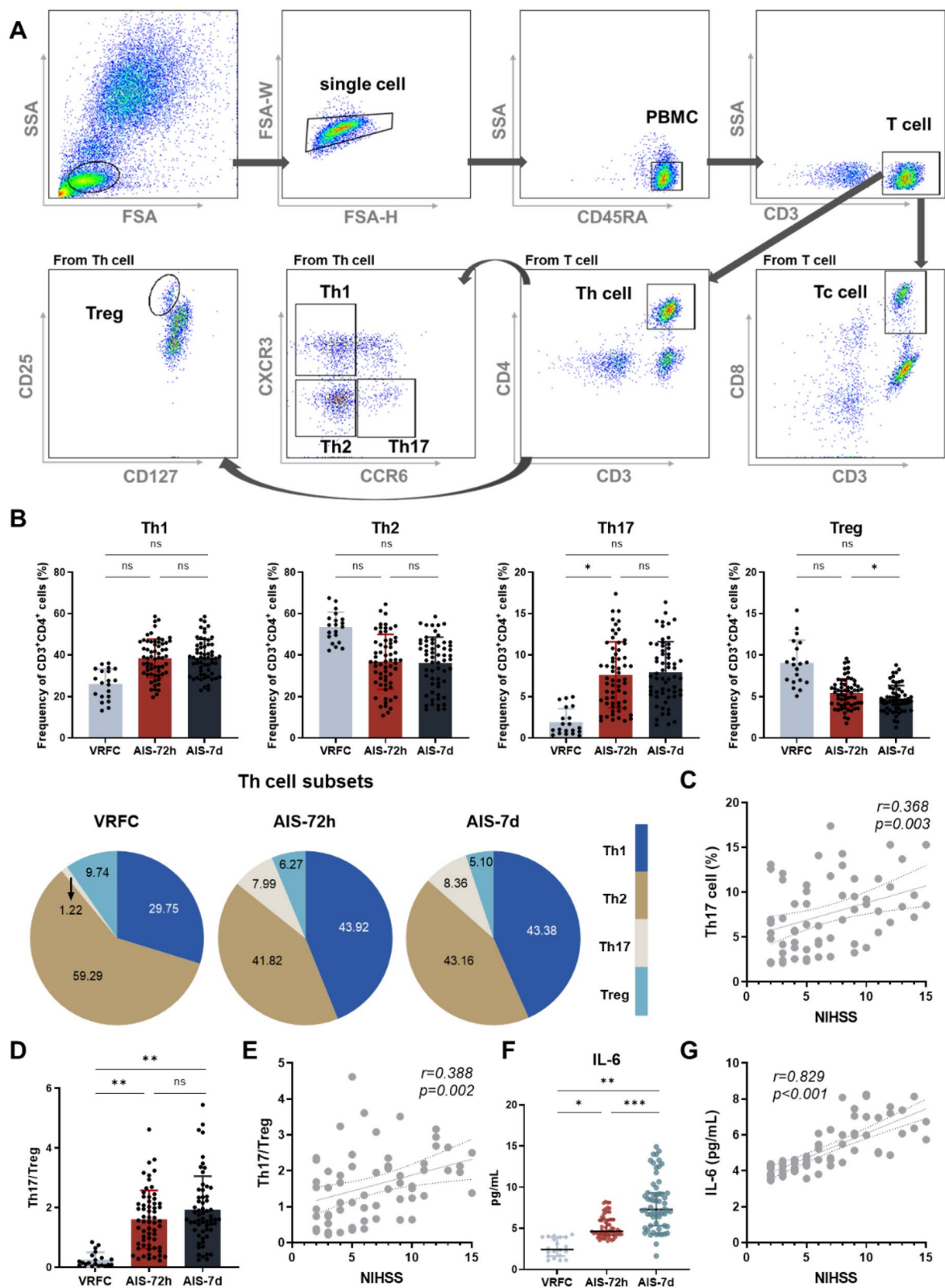
Fig. 1 (See legend on previous page.)

Chen *et al. Stem Cell Research & Therapy*   (2025) 16:134

Page 9 of 24

model: $T_N \rightarrow T_{CM} \rightarrow T_{EM} \rightarrow T_{EMRA}$ cells, eventually leading to cell death [63]. Therefore, our results demonstrate that stroke rapidly alters the composition of the circulating T-cell compartment, driving a shift toward a more activated and terminally differentiated state that reflects the dynamic changes in T-cell responses throughout AIS.

UMSCs modulate T-cell differentiation and cytokine secretion to restore immune homeostasis in LPS-induced post-stroke inflammation

Systemic inflammation following stroke can impair post-ischemic neurological recovery by enhancing sensitization to brain antigens, leading to increased brain T-cell infiltration and microvascular thrombosis [64]. UMSCs represent promising therapeutic targets for stroke treatment, as UMSC-mediated immune modulation has been shown to directly influence T lymphocyte differentiation and phenotype switching [29, 65]. To investigate whether UMSCs could protect against T-cell mediated post-stroke inflammation, PBMCs from AIS patients within 72 h of stroke onset were isolated and treated with LPS in vitro to mimic the systemic inflammatory sequelae of poststroke infection, as previously described [48]. These PBMCs were then cocultured with UMSCs in either a direct contact (CC) or indirect contact Transwell (TW) system for 72 h (Fig. 3A).

Flow cytometry and RT-qPCR were used to identify T-cell phenotypes (statistical data are shown in Table S7). Compared to the negative controls (without LPS stimulation), LPS did not affect the Th1 and Th2 cell populations ($p > 0.05$; Fig. 3C). However, LPS significantly increased the Th17 cell population ($p < 0.001$) while decreasing the Treg cell population ($p = 0.029$), thereby further enhancing the Th17/Treg cell imbalance ($p = 0.016$; Fig. 3C). In the CC coculture system, UMSCs reversed the T-cell differentiation bias by downregulating the Th17 cell population ($p < 0.001$) and upregulating Treg cells ($p < 0.001$), thus restoring the Th17/Treg balance ($p = 0.003$).

However, this reversal was lost in the TW coculture system, where a semi-permeable membrane barrier separated the PBMCs from the UMSCs (Fig. 3B, C; Table S7). As shown in Fig. 3D, RT-qPCR results of master transcription factors involved in T-cell differentiation confirmed the UMSC-mediated restoration of T-cell phenotypes [58]. In the CC coculture system, the mRNA expression of RORγt, associated with Th17 cells, was significantly downregulated ($p = 0.003$), while FOXP3, the key transcription factor for Treg cells, was upregulated ($p = 0.030$). The expression of T-bet, linked to Th1 cells, remained unchanged ($p = 0.059$), while GATA-3, associated with Th2 cells, was upregulated following direct coculture with UMSCs ($p = 0.019$).

We further quantified cytokine concentrations in the coculture system (statistical data are shown in Table S8). The results revealed that LPS significantly altered cytokine secretion in the PBMCs of AIS patients, leading to marked increases in IL-6 ($p < 0.001$; Fig. 3E), IL-17 ($p = 0.006$; Fig. 3G), TNF-α ($p = 0.011$; Fig. 3H), and IFN-γ ($p = 0.003$; Fig. 3I) compared to the negative control. UMSCs inhibited the LPS-induced increases in the IL-17 ($p = 0.018$), TNF-α ($p = 0.047$), and IFN-γ ($p = 0.047$) levels in the coculture microenvironment in the CC coculture system, but further elevated IL-6 levels in both the CC ($p = 0.032$) and TW ($p = 0.001$) coculture systems.

These results indicate that LPS disturbs the peripheral immune microenvironment in AIS patients, promoting a pro-inflammatory state by inducing Th/Treg imbalance and enhancing pro-inflammatory cytokine secretion. UMSCs help restore immune balance by inhibiting T-cell skewing toward Th17 differentiation and correcting the dysregulation of cytokine production (except for IL-6) in a contact-dependent manner.

To investigate whether the dramatic increase in IL-6 within the co-culture microenvironment has adverse effects on PBMCs, we conducted protein quantification analysis on PBMC proliferation, activation, inflammation,

(See figure on next page.)

Fig. 2 Characterization of T-cell compartment dynamics post-stroke and their correlations with stroke severity. **A** Representative FACS plots showing the flow cytometric gating strategy used to identify T-cell compartments, including T_N (CD45RA$^+$CCR7$^+$), T_{CM} (CD45RA$^-$CCR7$^+$), T_{EM} (CD45RA$^-$CCR7$^-$), and T_{EMRA} (CD45RA$^+$CCR7$^-$) cells within CD4$^+$ and CD8$^+$ cells. **B** Frequency and distribution of T cell compartments among CD4$^+$ T cells in VRFC and AIS patients. Data are represented as percentages of total CD4$^+$ T cells. The pie chart shows the mean relative proportions of different T cell compartments within the CD4$^+$ T cell population in VRFC and AIS patients. Correlation plots of the baseline CD4$^+$ T_N (**C**) and CD4$^+$ T_{EM} (**D**) cell frequency with NIHSS score. **E** Frequency and distribution of T cell compartments among CD8$^+$ T cells in VRFC and AIS patients. Data are represented as percentages of total CD8$^+$ T cells. The pie chart shows the mean relative proportions of different T cell compartments within the CD8$^+$ T cell population in VRFC and AIS patients. **F** Correlation plots of the baseline CD8$^+$ T_N cell frequency with NIHSS score. Data in **B** and **E** are presented as scatter plots showing mean values with SD. For correlations, the regression line and standard error are shown. Statistical comparisons between AIS and VRFC patients were performed via generalized linear models (age, sex, smoking, drinking, hypertension, and diabetes mellitus were included in the model during analysis). Statistical comparisons between baseline and 7-day data among AIS patients were made using the Mann–Whitney U test. Correlation analysis was conducted with Spearman's rank correlation test. p values < 0.05 are considered statistically significant. ns indicates not significant or $p \geq 0.05$; *$p < 0.05$, **$p < 0.01$, and ***$p < 0.001$. Abbreviations: T_{EMRA} cell, terminally differentiated effector memory T cell; T_{EM} cell, effector memory T cell; T_{CM} cell, central memory T cell; T_N cell, naïve T cell
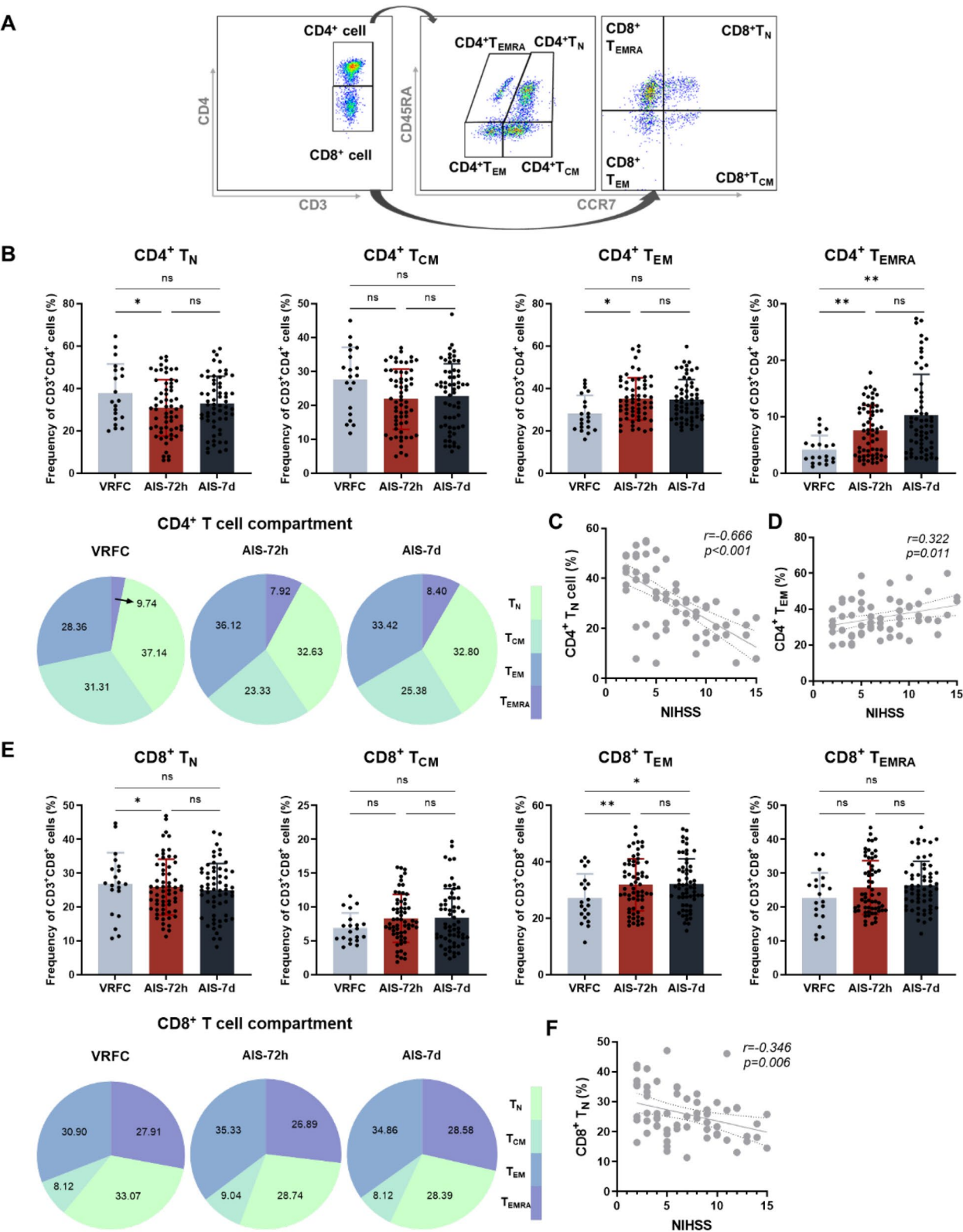
Fig. 2 (See legend on previous page.)

Chen *et al. Stem Cell Research & Therapy*   (2025) 16:134

Page 11 of 24

and the IL-6 downstream signaling molecule, signal transducer and activator of transcription 3 (STAT3) (Fig. S4B–D). Consistent with the increase in soluble IL-6, LPS stimulation upregulated IL-6 expression in PBMCs. Interestingly, when UMSCs were cultured alone in immune cell media, they responded to LPS stimulation by secreting soluble IL-6 (Fig. S4I). In line with our results, Cruz-Barrera et al. reported that UMSCs actively secrete IL-6 during PBMC inflammatory challenges [66]. Although IL-6 levels were further elevated in the presence of UMSCs, they did not exacerbate the pro-inflammatory responsed in PBMCs, evidenced by the downregulating of p-STAT3, cell proliferation marker proliferating cell nuclear antigen (PCNA), the early activation marker CD25, and the systemic inflammatory factor high-mobility group box 1 (HMGB1) upon UMSCs treatment (Figure S4E-G). Collectively, these results indicate that the increase in soluble IL-6 in the in vitro coculture system may result from the co-reactive secretion of PBMCs and UMSCs under LPS stimulation. While UMSCs alleviate LPS-induced pro-inflammatory effects, the precise role of IL-6 self-secretion in this immune context remains unclear and requires further investigation.

UMSCs rescue the broad T-cell compartment shift induced by LPS in AIS patients in a cell contact-dependent manner

To investigate whether UMSCs protect against shifts in the T-cell compartment, we analyzed the composition of T-cell compartments under different in vitro coculture systems (statistical data are shown in Table S7). As shown in Fig. 4, both $CD4^+$ and $CD8^+$ T-cell compartments underwent a broad shift from naive populations to more differentiated T_{EM} and T_{EMRA} cell phenotypes.

Specifically, in $CD4^+$ T-cells (Fig. 4A), LPS stimulation activated T_N and T_{CM} cells, driving their differentiation into effector populations, as evidenced by a significant decrease in T_N ($p=0.002$) and T_{CM} ($p<0.001$) cells and an increase in T_{EM} ($p<0.001$) and T_{EMRA} ($p<0.001$) cells. In the CC coculture system, UMSCs restored the balance of the T-cell compartments by preventing the activation and polarization of T_N ($p=0.001$) and T_{CM} ($p=0.001$) cells, leading to a reduction in the populations of T_{EM} ($p<0.001$) and T_{EMRA} cells ($p<0.001$). This effect was lost in the TW coculture system ($p>0.05$).

In $CD8^+$ T-cells, as shown in Fig. 4B, a similar trend was observed. $CD8^+$ T_N cells ($p<0.001$) decreased significantly, while T_{EM} cells increased ($p=0.001$) following LPS stimulation. No significant change was observed in $CD8^+$ T_{CM} ($p=0.853$) and T_{EMRA} cells ($p=0.917$). In the CC coculture system, as expected, UMSCs effectively corrected the imbalance in the $CD8^+$ T-cell compartment by downregulating the T_{EM} cells ($p<0.001$) and upregulating the T_N cells ($p<0.001$) However, this effect was absent in the TW coculture system.
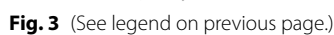
In summary, our results demonstrate that LPS can further mobilize T-cell reserves in the peripheral blood of AIS patients, promoting the differentiation of T_N cells into T_{EM} and T_{EMRA} cells. UMSCs effectively mitigate this shift and restore balance within the T-cell compartment through direct cell–cell interactions.

UMSCs protect against LPS-induced lymphocyte dysfunction through mitochondrial transfer and anti-oxidative stress

These findings suggest that UMSCs modulate the phenotype and function of LPS-induced PBMCs from AIS patients in a cell contact-dependent manner, although the underlying mechanism remains unclear. To further investigate how UMSCs protect against PBMC injury, we prestained UMSCs with the MitoTracker fluorescent probe and then cocultured them with unstained PBMCs for 72 h in both direct (CC) and indirect (TW) contact systems, as previously described [42]. After 72 h of ex vivo coculture, mitochondrial fluorescent signals from UMSCs were detected in PBMCs within the CC coculture system (Fig. 5A, B). This mitochondrial uptake was partially blocked when the cells were separated by a 0.4 μm membrane insert (Fig. 5A). To quantify mitochondrial transfer,

(See figure on next page.)

Fig. 3 UMSCs regulate LPS-induced Th-cell polarization and cytokine expression in PBMCs from AIS patients through a contact-dependent mechanism. **A** Schematic diagram of the ex vivo experimental setup. PBMCs were isolated from AIS patients within 3 d of stroke onset and then cocultured with UMSCs under LPS stimulation for 72 h. PBMCs and coculture supernatants were collected separately for cell phenotype identification and cytokine quantification. Experiments were conducted under both direct contact (CC) and indirect contact (TW) conditions (N=6/group). **B** Frequency and distribution of Th cell subsets under LPS stimulation and UMSCs coculture. Data are represented as percentages of total $CD4^+$ T cells. The pie chart shows the mean relative proportions of different Th cell subsets within the $CD4^+$ T cell population under different coculture conditions. **C** Th17/Treg cell ratio under various coculture conditions. **D** Expression levels of key genes involved in Th cell differentiation under CC coculture conditions. Concentration of IL-6 (**E**), IL-10 (**F**), IL-17 (**G**), TNF-α (**H**)**,** and IFN-γ (**I**) in different coculture systems. Statistical data are presented as scatter plots showing mean values with SD. Multiple data comparisons were performed using one-way ANOVA with the LSD post hoc test or Welch's t-test with Dunnett's post hoc test, while two-group comparisons were conducted using a t-test, with $p<0.05$ considered statistically significant. *$p<0.05$, **$p<0.01$, and ***$p<0.001$. Abbreviations: LPS, lipopolysaccharide; CC, contact coculture system; TW, Transwell coculture system; IFN-γ, interferon-gamma; TNF-α, tumor necrosis factor-alpha

Chen *et al. Stem Cell Research & Therapy*   (2025) 16:134

Page 12 of 24

Fig. 3 (See legend on previous page.)

Chen *et al. Stem Cell Research & Therapy*   (2025) 16:134

Page 13 of 24

CD3$^+$ T cells were gated, and the proportion of PBMCs with positive mitochondrial fluorescence was calculated. Following 72 h of coculture, 84.22% of the T cells in the CC system internalized UMSC-derived mitochondria, while only 31.13% of T cells in the TW system exhibited mitochondrial uptake (Fig. 5C). A significant difference in mitochondrial uptake between the two systems was observed ($p < 0.001$; Fig. 5C).

We used JC-1 and ROS assays to evaluate PBMC mitochondrial function. As shown in Fig. 5D, LPS significantly reduced MMP in PBMCs compared to the negative control ($p = 0.002$). This reduction was reversed when PBMCs were cocultured with UMSCs in the CC coculture system ($p < 0.001$); however, the reversal became ineffective in the TW coculture system ($p = 0.997$; Fig. 5E). Furthermore, as shown in Fig. 5F, LPS-treated PBMCs exhibited a dramatic increase in ROS expression in T cells ($p < 0.001$), with a corresponding increase in overall T-cell ROS expression levels ($p < 0.001$). However, this increase was significantly reduced when PBMCs were cocultured with UMSCs in the CC coculture system (ROS$^+$ T cell population: $p = 0.001$, ROS MFI: $p = 0.001$; Fig. 5G). No significant differences in ROS levels were observed between LPS-treated PBMCs and those in indirect contact with UMSCs (ROS$^+$ T cell population: $p = 0.471$, ROS MFI: $p = 0.842$; Fig. 5G).

Collectively, the direct interaction between UMSCs and PBMCs facilitates the internalization of UMSC-derived mitochondria into T cells, which is associated with improved MMP and reduced ROS production. These findings suggest that mitochondrial transfer from UMSCs plays a key role in their protective effects on PBMCs, although the underlying mechanisms remain to be fully elucidated.

UMSCs alleviate acute neurological deficits and peripheral immune dysregulation after ischemic stroke, with mitochondrial depletion abolishing these effects

To investigate the role of mitochondrial transfer in the protective effects of UMSCs, mtDNA depletion was achieved in UMSCs by treating them with the FDA-approved ddC, reducing their mtDNA content by 50–80% (Fig. 6A). Morphological changes in UMSC cells during mtDNA depletion are shown in Figure S5. As depicted in Fig. 6B, C57BL/6J mice underwent a 45-min ischemic stroke via MCAO, followed by reperfusion. Two hours post-reperfusion, the mice were randomly assigned to receive one of the following treatments via tail vein injection: 6×10^6/kg normal UMSCs, mtDNA-depleted UMSCs, or saline as a control. After 72 h, the mice were euthanized, and various endpoints were assessed. Statistical data are provided in Table S9-13.

UMSC treatment significantly reduced the infarct volume ($p = 0.017$, Fig. 6E) compared to control mice, whereas mtDNA-depleted UMSCs showed no significant effect ($p = 1.000$). The adoptive transfer of UMSCs also potentiated short-term sensorimotor function, as evidenced by a decreased Longa test score ($p = 0.003$, Fig. 6C) and an increased left forelimb touch frequency in the cylinder test ($p < 0.001$, Fig. 6D). In contrast, mtDNA-depleted UMSCs improved performance only in the cylinder test ($p < 0.001$, Fig. 6D) but had no effect on the Longa test score ($p = 1.000$, Fig. 6C), suggesting that mitochondrial transfer plays an important role in functional recovery. Additionally, stroke-induced reduction in spleen weight was observed in MCAO mice ($p < 0.001$, Fig. 6F), a sign of immune suppression often associated with ischemic stroke. UMSC treatment mitigated this reduction ($p < 0.001$), whereas mtDNA depletion abolished this effect ($p = 0.837$).

T-cell phenotypes and cytokine production were also assessed in MCAO mice. While the total T cell proportion remained unchanged (Fig. S6A), the proportion of Th cells significantly decreased ($p = 0.004$, Fig. 6G), whereas Tc cells increased ($p = 0.001$) at day 3 post-stroke. UMSC treatment did not significantly alter the proportions of Th and Tc cells ($p > 0.05$), but significantly reduced the elevated Th17 ($p = 0.004$) and Treg ($p = 0.003$) cell populations (Fig. 6H). Unlike in AIS patients, the Th17/Treg ratio did not change following UMSC treatment ($p > 0.05$, Fig. 6I). Consistent with findings in AIS patients, levels of other cytokines in the peripheral blood of mice remianed unchanged ($p > 0.05$, Figure S6B-G), except for IL-6, which was significantly upregulated following ischemic stroke ($p = 0.007$). UMSC treatment reduced IL-6 levels ($p = 0.016$), an effect that was reversed by mtDNA depletion ($p = 0.992$, Fig. 6J).

(See figure on next page.)

Fig. 4 UMSCs target LPS-induced T-cell compartments shift in PBMCs from AIS patients. Frequency and distribution of T cell compartments among CD4$^+$ (**A**) and CD8$^+$ (**B**) T cells under various coculture conditions. Data are represented as percentages of total CD4$^+$ (**A**) and CD8$^+$ (**B**) T cells. The pie charts show the mean relative proportions of different T cell compartments within the CD4$^+$ (**A**) and CD8$^+$ (**B**) T cell populations across different coculture systems. Statistical data are presented as scatter plots with mean values and SD. Comparisons were performed using one-way ANOVA with the LSD post hoc test or Welch's t-test with Dunnett's post hoc test, with $p < 0.05$ considered statistically significant. *$p < 0.05$, **$p < 0.01$, and ***$p < 0.001$
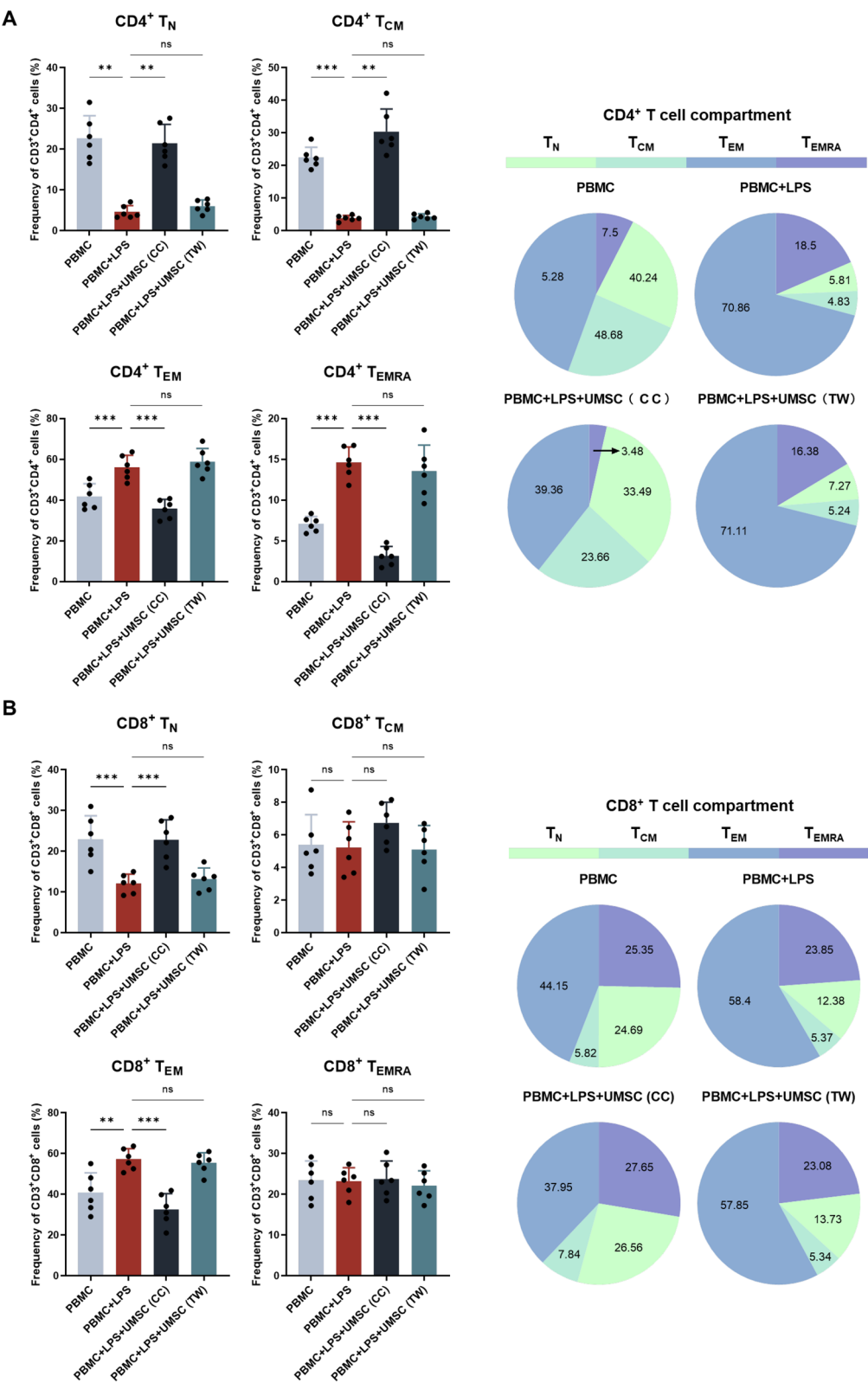
Fig. 4 (See legend on previous page.)

Additionally, ischemic stroke-induced oxidative stress in peripheral blood T cells of mice, as evidenced by a significant upregulation in both the proportion ($p = 0.005$) and expression levels ($p = 0.010$) of ROS-expressing cells (Fig. 6K). UMSC treatment inhibited this oxidative stress (ROS$^+$ T cell population: $p = 0.008$; ROS MFI: $p = 0.047$), but this protective effect was lost following mtDNA depletion ($p > 0.05$, Fig. 6K).

Taken together, our results indicate that mitochondrial depletion abolishes the protective effects of UMSCs on both brain injury and the peripheral immune dysregulation following MCAO.

Mitochondrial depletion inhibits UMSC-mediated reversal of the T-cell compartment shift in ischemic stroke mice

To confirm the effect of UMSCs in vivo administration on the dynamic differentiation of peripheral T cells following ischemic stroke, we analyzed the composition of T cell compartments in the peripheral blood of mice. The proportions of T_N, T_{CM}, T_{EM} cells, and T_{EX} cells were detected by flow cytometry, with statistical data summarized in Table S12. As shown in Fig. 7, consistent with clinical data, both CD4$^+$ and CD8$^+$ T-cell compartments in ischemic stroke mice underwent a shift from the naïve population to memory or effector populations.

Specifically, in CD4$^+$ T cells (Fig. 7A), the MCAO group showed a significant decrease in T_N cells compared to the sham group ($p = 0.046$), while the proportions of T_{CM} ($p = 0.025$), T_{EM} ($p = 0.002$), and T_{EX} ($p < 0.001$) cells were significantly increased. UMSC treatment effectively reversed this shift, as indicated by the significant downregulation of T_{EM} ($p = 0.012$) and T_{EX} cells ($p = 0.001$), along with a significant increase in the T_N ($p = 0.021$) cell population. While not statistically significant compared to the MCAO group, UMSC treatment induced a trend toward decreasing T_{CM} cell populations ($p = 0.925$).

Notably, this effect was abolished when mtDNA was depleted in UMSCs.

A similar pattern was observed in CD8$^+$ T cells (Fig. 7B), where ischemic stroke caused a significant decrease in the T_N cell population ($p = 0.022$) and an increase in T_{EM} ($p = 0.038$) and T_{EX} ($p < 0.001$) cell populations. UMSC treatment partially reversed this shift, particularly by significantly downregulating T_{EX} cells ($p < 0.001$) and upregulating T_N cells ($p = 0.028$). However, when mtDNA was depleted in UMSCs, the effects were lost.

Overall, our findings demonstrate that UMSC treatment effectively mitigates peripheral immune dysregulation following ischemic stroke by reversing the shift in T-cell compartments, with mitochondrial function playing a pivotal role in their therapeutic efficacy.

Discussion

Emerging research highlights that peripheral inflammation-mediated secondary injury offers significant potential as a target for stroke treatment. UMSCs hold promise by mitigating progressive inflammation both centrally and peripherally, thereby addressing the broader pathological scope of stroke and extending the therapeutic window beyond traditional brain-focused approaches. Here, we investigated the T-cell response following ischemic stroke and explored the therapeutic potential of UMSCs, focusing on mitochondria-mediated rescue of the T-cell phenotype. This is the first study to demonstrate mitochondrial transfer from UMSCs to peripheral T cells, effectively reversing T-cell compartment shifts and alleviating oxidative stress. Our findings advance the novel strategy of UMSC-mediated T-cell metabolic reprogramming, offering a protective peripheral immune environment to support brain repair in ischemic stroke.

(See figure on next page.)

Fig. 5 UMSCs transfer mitochondria to PBMCs in AIS patients and restore their mitochondrial function. PBMCs were isolated from AIS patients within 3 d of stroke onset and cocultured with MitoTracker-labeled UMSCs under LPS stimulation ex vivo for 72 h. The effects of UMSCs on MMP and ROS levels in PBMCs were assessed via JC-1 and ROS staining. Experiments were conducted under both direct contact (CC) and indirect contact (TW) conditions (N = 6/group). **A**, **B** Representative images of PBMCs following mitochondrial transfer in the coculture system. Violet: MitoTracker; blue: DAPI (cell nuclei); scale bars: 20 and 50 μm. **B** Merged image of stained exogenous mitochondria overlaid with visible microscopy under the CC coculture system. The black arrow indicates UMSCs, and the white arrow indicates PBMCs. **C** Representative flow cytometry plots and statistical graphs of mitochondrial fluorescence expression in T cells. **D** Fluorescence microscopy of PBMCs stained with JC-1 after coculture. The images depict JC-1 aggregates (red fluorescence), JC-1 monomers (green fluorescence), and merged images. The accumulation of JC-1 dye in the mitochondrial matrix results in red fluorescence; as the MMP decreases, JC-1 remains in its monomeric form, producing green fluorescence. **E** Quantified JC-1 fluorescence intensity data obtained through flow cytometry. **F** Fluorescence microscopy of PBMCs stained for ROS after coculture. The images show ROS (green fluorescence), DAPI (blue fluorescence), and merged images. **G** ROS levels measured by flow cytometry, presented as the percentage of ROS-positive cells (left) and the fluorescence intensity of ROS (right). Statistical data are presented as scatter plots with mean values and SD. T-tests (**C**) and the Welch T-test with Dunnett's post hoc test (**E, G**) were used for group comparisons, with $p < 0.05$ considered statistically significant. ns indicates not significant or $p \geq 0.05$; *$p < 0.05$, **$p < 0.01$, and ***$p < 0.001$. Abbreviations: Pos: LPS stimulated; Neg: negative stimulated; Ctrl: control group (without UMSCs); ROS, reactive oxygen species; MFI, mean fluorescence intensity
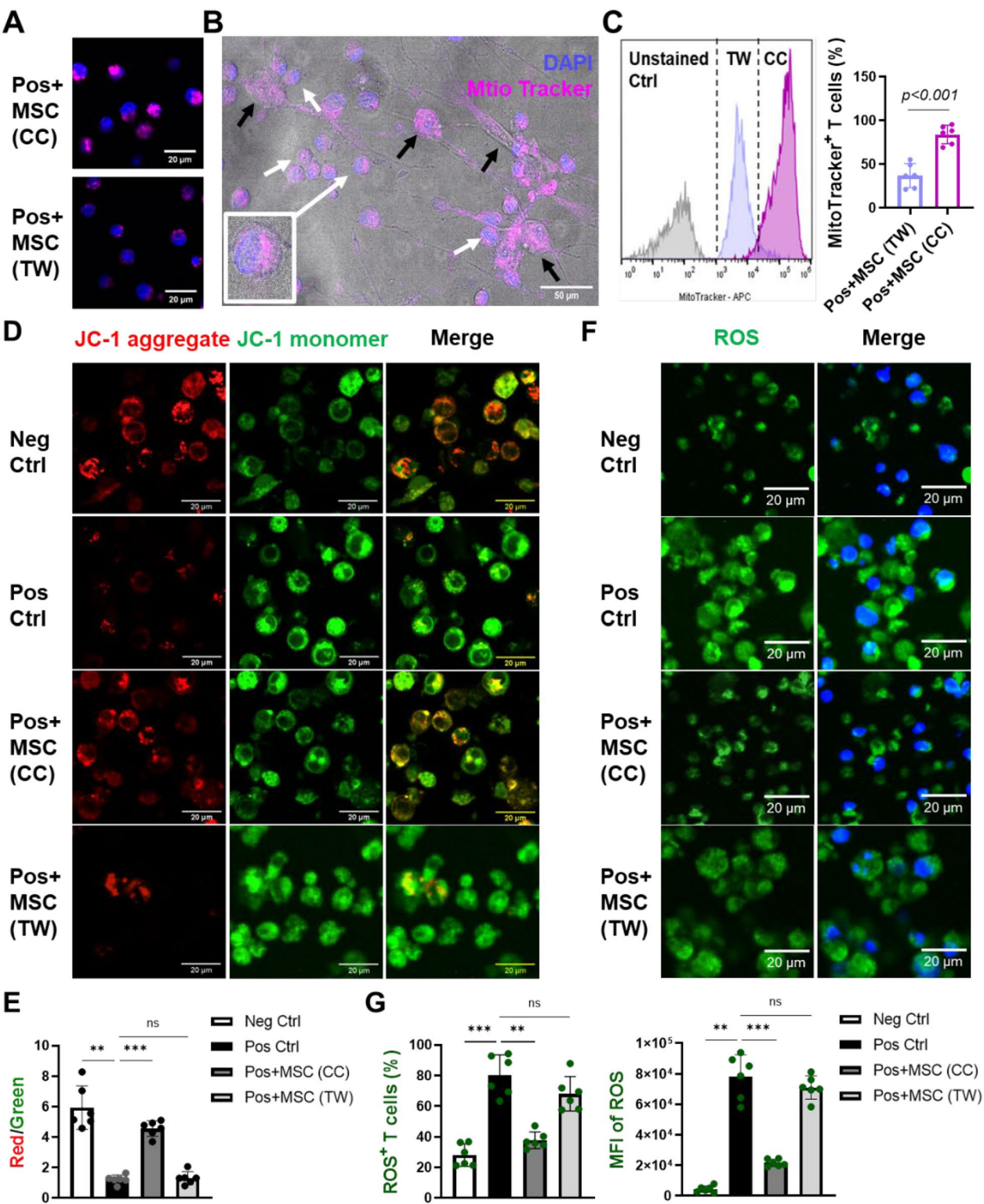
Fig. 5 (See legend on previous page.)

First, we characterized the T-cell compartments in ischemic stroke patients and mice. Following a cerebral ischemic attack, T cells react to danger-associated molecular patterns released by dead neurons through antigen-dependent antigen recognition and display an activated phenotype [27]. T_N cells are the source of an antigen-specific T-cell after antigen priming and once activated, they differentiate into T_{EM} and T_{EMRA}, leading to the increase of immunodominant central nervous system antigen-specific T-cells [24]. Chronic infection and persistent antigen stimulation impair lymphocyte function, leading to the acquisition of an exhausted phenotype [16]. The early activation of $CD4^+$ T_N and T_{CM} cells increases the risk of infection and is associated with worse outcomes [67], potentially contributing to stroke-induced immunosuppression (SIIS), a neuroimmune imbalance characterized by an early loss and functional deactivation of T cells [61]. Zhang et al. reported the increased expression of inhibitory receptors PD-1 on activated $CD4^+$ T cells in the stable phase (defined as 10–30 days post-IS) [25]. Consistent with these studies, we observed a significant decrease in both $CD4^+$ and $CD8^+$ T_N cell populations in the peripheral blood of ischemic stroke patients and mice, which correlated with stroke severity in patients. In contrast, T_{EM} and T_{EMRA} cells in patients, as well as PD-1 high-expression T_{EX} cells in mice, significantly increased, with the increase in patients persisting up to 7 days post-stroke. In addition, we observed significant atrophy of the spleen-the largest peripheral immune organ in MCAO mice, indicating a marked loss of adaptive immune cells following stroke [68]. Our results suggest that stroke triggers the activation of T_N cells and skew T-cell compartments, leading to a significant increase in terminally exhausted phenotypes, which may elevate the risk of SIIS.

In addition, the shift of T-cell compartments is always accompanied by specific increases in Th1 and Th17 cells and activated Treg cells in $CD4^+$ T cells in ischemic stroke patients and mice [69, 70]. Th17 cells specifically produce IL-17, playing a crucial role in pro-inflammatory effects, activating chemotaxis-related genes in microglia, and exacerbating neurological deficits [71]. In contrast, Treg cells express IL-10, shifting microglia gene expression toward a pro-regenerative function and enhancing microglial repair activity [72–75]. Moreover, Th17/Treg imbalance has been associated with impaired immune responses and increased susceptibility to infections post-stroke [60]. Importantly, Treg and Th17 cells share a close developmental relationship, both originating from naïve T cells and relying on the TGF-β signaling pathway for initial differentiation [76]. TGF-β alone promotes Treg differentiation, while the presence of IL-6 activates STAT3, driving T cells preferentially toward Th17 differentiation and further supporting Th17 cell expansion [77]. Consistent with previous studies, we observed a peripheral Th17/Treg imbalance [78] and upregulation of IL-6 [79, 80], both of which correlate with stroke severity, underscoring the importance of the Th17/Treg balance as a peripheral immune marker and therapeutic target for neuroinflammation in AIS.

UMSC transplantation exerts a neuroprotective effect in AIS by alleviating the peripheral inflammatory environment and promoting Treg cell expansion [28, 32, 68, 81]. Initially attributed to "bystander" effects, the robust anti-inflammatory and immunomodulatory properties of UMSCs following systemic delivery are now believed to be primarily mediated through mitochondrial transfer. Activated CD4+T cells rapidly adhere to MSCs, which transfer mitochondria to these activated T cells, resulting in the suppression of Th1 and Th17 responses while promoting the expansion of a highly suppressive Treg cell population [38–42]. Additionally, mitochondrial transfer facilitates the conversion of Th17 cells into Treg cells, thereby re-establishing the Th17/Treg balance [82]. Furthermore, MSC-derived mitochondria reduce

(See figure on next page.)

Fig. 6 Mitochondrial depletion abolishes the therapeutic effect of UMSCs on neurological deficits and peripheral immune microenvironment in MCAO mouse models. **A** RT-qPCR analysis of mtDNA expression in UMSCs during ddC depletion. **B** Experimental design for UMSCs treatment in experimental ischemic stroke. The experiment included four groups: sham surgery, MCAO, MCAO+UMSC treatment, and MCAO+UMSC (ddC) treatment (N=5/group). Brain tissues were collected for TTC staining, spleens were harvested and weighed, and peripheral T cells and plasma were isolated for T cell phenotype and cytokine analysis. Data are presented as scatter plots with median values and IQR. Severity and recovery of sensorimotor deficits after cerebral focal ischemia were assessed using the Longa test (**C**) and cylinder test (**D**). (**E**) TTC staining of brain slices 3 days post-ischemia (white indicates the infarct area), with quantification of infarct volume based on relative proportion from TTC staining. **F** Comparison of spleen weights across different treatment groups. **G** Representative flow plot and frequencies of T cell subsets in different treatment groups, expressed as percentages of total $CD45^+$ cells. **H** Representative flow plot and frequencies of Th17 and Treg cells, expressed as percentages of total $CD4^+$ T cells. **I** Comparison of Th17/Treg cell ratio among groups. **J** IL-6 concentration in different mouse model groups. **K** Flow histogram and ROS expression in total T cell across different groups. Except for additional annotations, data are presented as scatter plots with mean values and SD. Statistical comparisons were performed using repeated measures analysis of variance, one-way ANOVA with Tukey's post hoc test, Welch's t-test with Dunnett's post hoc test, or the Kruskal–Wallis test, with $p < 0.05$ considered statistically significant. *$p < 0.05$, **$p < 0.01$, and ***$p < 0.001$. Abbreviations: mtDNA, mitochondrial DNA; MCAO, middle cerebral artery occlusion
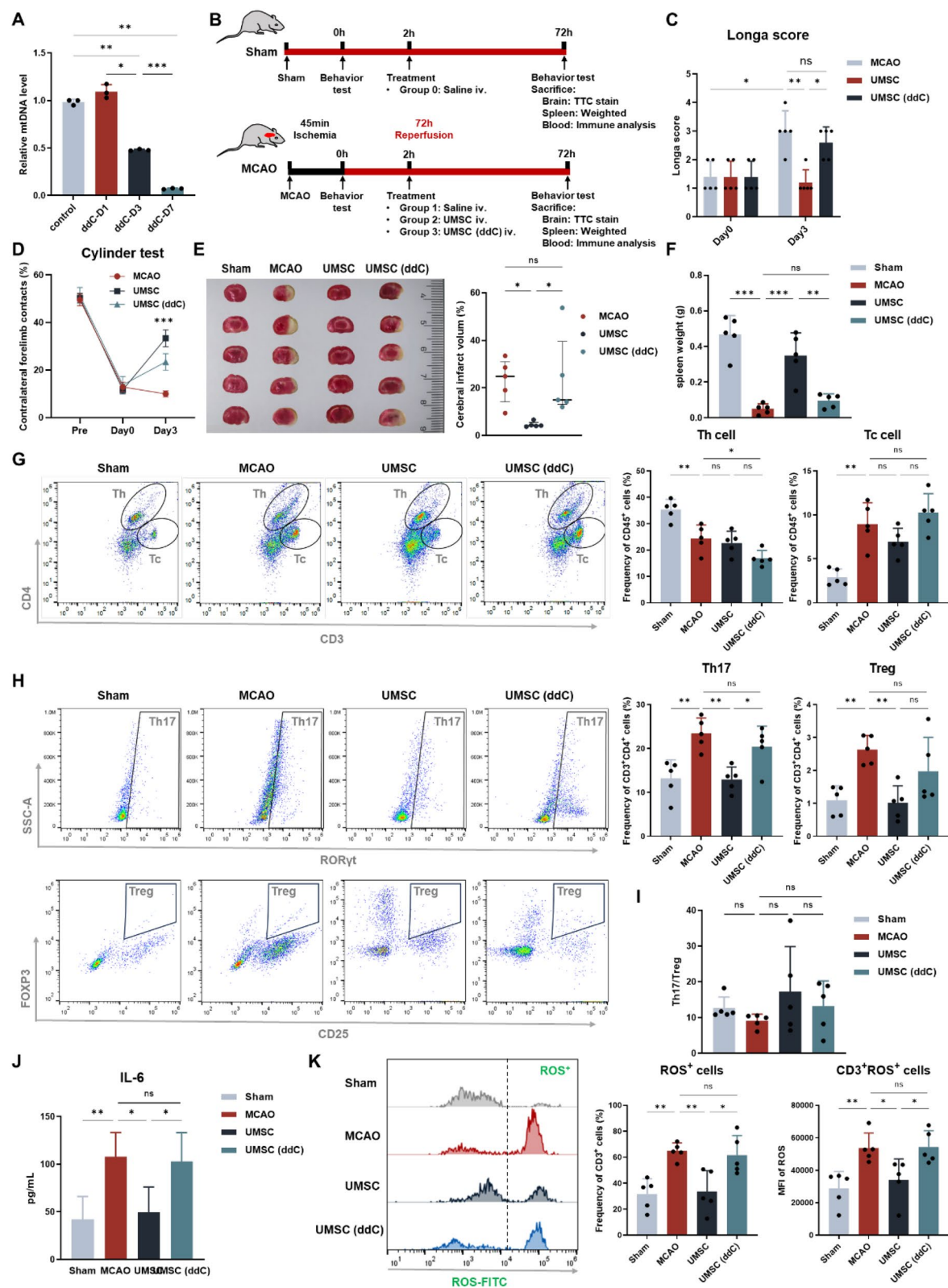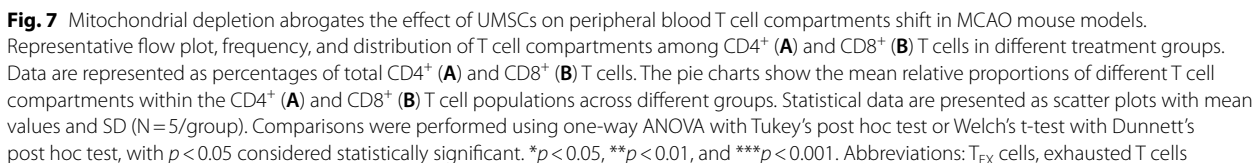
Chen *et al. Stem Cell Research & Therapy* (2025) 16:134

Page 18 of 24

Fig. 6 (See legend on previous page.)

Fig. 7 Mitochondrial depletion abrogates the effect of UMSCs on peripheral blood T cell compartments shift in MCAO mouse models. Representative flow plot, frequency, and distribution of T cell compartments among CD4+ (**A**) and CD8+ (**B**) T cells in different treatment groups. Data are represented as percentages of total CD4+ (**A**) and CD8+ (**B**) T cells. The pie charts show the mean relative proportions of different T cell compartments within the CD4+ (**A**) and CD8+ (**B**) T cell populations across different groups. Statistical data are presented as scatter plots with mean values and SD (N = 5/group). Comparisons were performed using one-way ANOVA with Tukey's post hoc test or Welch's t-test with Dunnett's post hoc test, with $p < 0.05$ considered statistically significant. *$p < 0.05$, **$p < 0.01$, and ***$p < 0.001$. Abbreviations: T_{EX} cells, exhausted T cells

Chen *et al. Stem Cell Research & Therapy*   (2025) 16:134

Page 20 of 24

the production of pro-inflammatory cytokines, including IL-17, TNF-α, and IFN-γ, in T cells [83, 84]. Mitochondrial transfer from MSCs has also been shown to attenuate hypoxia–ischemia-induced mitochondrial dysfunction in PC12 cells [36], reduce ROS levels in neural cells, and improve cell survival in MCAO mice [85]. In line with this research, our findings indicate that UMSC-mediated protection in ischemic stroke operates through both central and peripheral mechanisms. Centrally, UMSC treatment provides neuroprotection and facilitates neural recovery in the MCAO mouse model. Peripherally, UMSCs alleviate LPS-induced exacerbation of stroke-primed T-cell response ex vivo by reversing the skewing of T_N and T_{CM} cells toward T_{EMRA} and T_{EM} cells and restoring the Th17/Treg imbalance, accompanied by immune resolution by downregulation proinflammatory IL-17, TNF-α, and IFN-γ. This immune modulation is further verified in vivo in MCAO mice. Notably, blocking direct contact between UMSCs and T cells using a semi-permeable membrane in vitro, as well as knocking out mtDNA in UMSCs in vivo, abolishes the therapeutic effects of UMSCs, highlighting the crucial role of mitochondrial transfer in UMSC-mediated protection against ischemic stroke.

Our prior studies have suggested that neural stem cell-derived organelles could mimic respiration chain function and rectify excessive mitochondrial ROS production [86], which prompted us toinvestigate whether UMSCs similarly affect T cell mitochondrial function, thereby driving T cell dynamics. Emerging research underscores the critical role of cellular energy metabolism and ROS synthesis in T-cell activation and differentiation [87]. Naïve T cells are metabolically quiescent, but undergo metabolic reprogramming upon activation, shifting from OXPHOS to aerobic glycolysis until sufficient differentiation occurs to support effector function [88]. Fully differentiated inflammatory Th17 cells primarily rely on glycolysis, while Treg cells depend more on the tricarboxylic acid (TCA) cycle [89]. Mitochondria not only serve as the energy factory for the TCA cycle and OXPHOS but also constitute the main cellular source of ROS synthesis [90]. Mitochondrial-derived ROS function as signaling molecules that influence T-cell fate and function. While moderate ROS levels facilitate naïve T-cell activation, chronic antigen stimulation leads to mitochondrial dysfunction and excessive ROS production, driving T-cell exhaustion rather than memory formation; reducing ROS levels mitigates this effect [91, 92]. Furthermore, enhanced ROS synthesis stabilizes the transcription factor RORγt, promoting Th17 differentiation [93], and boosting proinflammatory cytokines expression [94]. Previous studies by Zhang et al. [95] and Wang et al. [96] have demonstrated that cerebral ischemia induces glycolysis in peripheral CD4$^+$ T cells, contributing to Th17/Treg imbalance, and that targeting key regulators in metabolic pathways can reverse these effects and improve stroke recovery. Thus, mitochondrial metabolism and ROS levels critically regulate T-cell compartmental dynamics and the Th17/Treg balance. In our study, we found that UMSCs transfer mitochondria to T cells, reducing oxidative stress and restoring the MMP in activated T cells. These findings were further validated in MCAO mice, where the therapeutic effects of UMSCs were abolished upon mitochondrial depletion. Building upon these insights, our results highlight mitochondrial transfer as a key mechanism underlying the immunomodulatory effects of UMSCs, with metabolic reprogramming likely playing a pivotal role in UMSC-mediated T-cell protection in AIS patients.

The limitations of this study are as follows: First, the sample size of AIS patients is relatively small. Future studies should include a larger cohort and stratify by gender, age, and disease severity to provide a more comprehensive and detailed understanding of peripheral immune profile changes in stroke patients. Second, the mechanisms underlying UMSC-mediated T-cell immune regulation remain insufficiently explored. Given that T cells are highly dynamic and heterogeneous, with metabolic adaptations involving throughout the process from activation to exhaustion, further studies are needed to elucidate the pathways involved in mitochondrial transfer and regulation. This includes investigating key signaling molecules, mitochondrial biogenesis, and the role of oxidative stress. Finally, additional in vivo experiments are necessary to determine the optimal UMSCs dosage required for effective mitochondrial transfer to T cells and the subsequent modulation of immune functions.

Graphic abstract

Following acute ischemic stroke (AIS), T cells are exposed to persistent antigens and inflammatory signals, leading to the activation of T_N cells into effector and memory T cells. Effector T cells then differentiate into various subsets, resulting in an imbalance in the Th17/Treg ratio. This imbalance is accompanied by elevated IL-6 levels, which correlate with disease severity and play a crucial role in the progression of acute cerebral ischemia. The exposure of primed T cells to LPS further exacerbates T_N cell mobilization, shifting T-cell compartments toward T_{EMRA} and T_{EM} cells. This process drives effector T cells toward Th17 differentiation, aggravating the Th17/Treg imbalance, and disrupting the peripheral immune microenvironment, as evidenced by the upregulation of IL-6, IL-17, IFN-γ, and TNF-α. UMSCs, in response to the LPS-induced poststroke inflammatory state, can inhibit excessive T_N cell mobilization, prevent differentiation

Chen *et al. Stem Cell Research & Therapy*   (2025) 16:134

Page 21 of 24

bias within the T-cell compartment and effector T cells, and correct the disrupted peripheral immune microenvironment. Although UMSCs secrete IL-6 during this process, leading to a cascade increase in IL-6 levels, this does not promote Th17 cell differentiation. Instead, UMSCs transfer mitochondria to LPS-induced PBMCs, reducing oxidative stress and restoring the mitochondrial membrane potential (MMP), suggesting that mitochondrial transfer is a key mechanism underlying the immunomodulatory effects of UMSCs, with metabolic reprogramming likely contributing to T-cell protection in AIS patients.

Conclusion

In conclusion, this study highlights the complex immune dysregulation following AIS and demonstrates the therapeutic potential of UMSCs in restoring immune balance, mitigating inflammation, and enhancing mitochondrial function in stroke patients. Further research is warranted to elucidate the precise mechanisms underlying UMSC-mediated immunomodulation and to assess their clinical applicability in stroke treatment.

Abbreviations

AIS	Acute ischemic stroke
VRFC	Vascular risk factor controls
NIHSS	National Institutes of Health Stroke Scale
UMSCs	Umbilical mesenchymal stem cells
PBMC	Peripheral blood mononuclear cell
Th cell	Helper T cell
Tc cell	Cytotoxic T cell
Treg cell	Regulatory T cell
T_{EMRA} cell	Terminally differentiated effector memory T cell
T_{EM} cell	Effector memory T cell
T_{CM} cell	Central memory T cell
T_N cell	Naïve T cell
T_{EX} cell	Exhausted T cell;
IL	Interleukin
IFN-γ	Interferon γ
TNF-α	Tumor necrosis factor α
CC	Contact co-culture system
TW	Transwell co-culture system
LPS	Lipopolysaccharide
MCAO	Middle cerebral artery occlusion
mtDNA	Mitochondrial DNA
ROS	Reactive oxygen species
MMP	Mitochondrial membrane potential
ddC	2′,3′-Dideoxycytidine

Supplementary Information

The online version contains supplementary material available at https://doi.org/10.1186/s13287-025-04224-6.

Additional file 1.

Additional file 2.

Additional file 3.

Author contributions

JL contributed to the conception and revision of the manuscript. SN–C performed the experimental work; designed the experiments; acquired, analyzed, and interpreted the data; and drafted and revised the manuscript. CH contributed to the design of the experiments, interpreted the data, and revised the manuscript. ZH-S performed the immunofluorescence staining. XG provided human-derived umbilical cord mesenchymal stem cells. LY-C participated in the screening and enrollment of patients. LW contributed to the interpretation of the data. WZ contributed to the conception of the manuscript and interpreted the data. All the authors read and approved the final manuscript.

Availability of data and materials

All additional files are included in the manuscript. The data of this study are available from the corresponding author upon reasonable request.

Declarations

Ethics approval and consent to participate

This study was conducted at the Stem Cell Clinical Research Center of the First Affiliated Hospital of Dalian Medical University. The study, titled "Clinical Study of Umbilical Cord Mesenchymal Stem Cell Therapy for Acute Ischemic Stroke" (No. YJ-GXB-2022-01, January 16, 2022), received ethical approval from the Ethics Committee of the First Affiliated Hospital of Dalian Medical University. The approval encompassed the isolation and preparation of human umbilical cord mesenchymal stem cells, the recruitment of patients with acute ischemic stroke, and the collection of their biological samples for research purposes. Written informed consent was obtained from all patients or their legally authorized representatives. The animal studies were approved by the Ethics Committee of the Animal Experiment Center of Dalian Medical University and conducted in accordance with the *Guide for the Care and Use of Laboratory Animals* of the National Institutes of Health. The approved project was titled "Investigation of the Effects of Stem Cells and Engineered Vesicles on Neurological Repair in Ischemic Stroke" (No. AEE23127, February 28, 2023). In addition, this work has been reported in line with the ARRIVE guidelines 2.0. There were no ethical conflicts associated with this manuscript.

Consent for publication

Not applicable.

Artificial intelligence (AI)

The authors declare that they have not use AI-generated work in this manuscript" in this section.

Competing interests

The authors declare that they have no competing interests.

Author details

[1]Stem Cell Clinical Research Center, National Joint Engineering Laboratory, Regenerative Medicine Center, The First Affiliated Hospital of Dalian Medical University, Dalian, People's Republic of China. [2]Dalian Innovation Institute of Stem Cell and Precision Medicine, Dalian, People's Republic of China. [3]Department of Neurology, The First Affiliated Hospital of Dalian Medical University, Dalian, People's Republic of China. [4]College of Integrated Chinese and Western Medicine, Dalian Medical University, Dalian, People's Republic of China.

References

1. Feigin VL, Stark BA, Johnson CO, Roth GA, Bisignano C, Abady GG, et al. Global, regional, and national burden of stroke and its risk factors,

Chen *et al. Stem Cell Research & Therapy*   (2025) 16:134

Page 22 of 24

1990–2019: a systematic analysis for the Global Burden of Disease Study 2019. Lancet Neurol. 2021;20(10):795–820.

2. Tu W-J, Wang L-D. China stroke surveillance report 2021. Mil Med Res. 2023;10(1):33.

3. Aguiar d -Sousa D, von Martial R, Abilleira S, Gattringer T, Kobayashi A, Gallofré M, et al. Access to and delivery of acute ischaemic stroke treatments: A survey of national scientific societies and stroke experts in 44 European countries. Eur Stroke J. 2019;4(1):13–28.

4. Phipps MS, Cronin CA. Management of acute ischemic stroke. BMJ. 2020;368:l6983.

5. Wassélius J, Arnberg F, von Euler M, Wester P, Ullberg T. Endovascular thrombectomy for acute ischemic stroke. J Intern Med. 2022;291(3):303–16.

6. Endres M, Moro MA, Nolte CH, Dames C, Buckwalter MS, Meisel A. Immune pathways in etiology, acute phase, and chronic sequelae of ischemic stroke. Circ Res. 2022;130(8):1167–86.

7. Duan M, Xu Y, Li Y, Feng H, Chen Y. Targeting brain-peripheral immune responses for secondary brain injury after ischemic and hemorrhagic stroke. J Neuroinflamm. 2024;21(1):102.

8. Iadecola C, Buckwalter MS, Anrather J. Immune responses to stroke: mechanisms, modulation, and therapeutic potential. J Clin Invest. 2020;130(6):2777–88.

9. Fury W, Park KW, Wu Z, Kim E, Woo M-S, Bai Y, et al. Sustained increases in immune transcripts and immune cell trafficking during the recovery of experimental brain ischemia. Stroke. 2020;51(8):2514–25.

10. Zhang D, Ren J, Luo Y, He Q, Zhao R, Chang J, et al. T Cell Response in ischemic stroke: from mechanisms to translational insights. Front Immunol. 2021;12:707972.

11. Gelderblom M, Leypoldt F, Steinbach K, Behrens D, Choe C-U, Siler DA, et al. Temporal and spatial dynamics of cerebral immune cell accumulation in stroke. Stroke. 2009;40(5):1849–57.

12. Feng Y, Liao S, Wei C, Jia D, Wood K, Liu Q, et al. Infiltration and persistence of lymphocytes during late-stage cerebral ischemia in middle cerebral artery occlusion and photothrombotic stroke models. J Neuroinflamm. 2017;14(1):248.

13. Zheng Y, Ren Z, Liu Y, Yan J, Chen C, He Y, et al. T cell interactions with microglia in immune-inflammatory processes of ischemic stroke. Neural Regen Res. 2025;20(5):1277–92.

14. Shi L, Sun Z, Su W, Xu F, Xie D, Zhang Q, et al. Treg cell-derived osteopontin promotes microglia-mediated white matter repair after ischemic stroke. Immunity. 2021;54(7):15275.

15. Qiu Y-M, Zhang C-L, Chen A-Q, Wang H-L, Zhou Y-F, Li Y-N, et al. Immune cells in the BBB disruption after acute ischemic stroke: targets for immune therapy? Front Immunol. 2021;12:678744.

16. Chapman NM, Boothby MR, Chi H. Metabolic coordination of T cell quiescence and activation. Nat Rev Immunol. 2020;20(1):55–70.

17. Davenport MP, Smith NL, Rudd BD. Building a T cell compartment: how immune cell development shapes function. Nat Rev Immunol. 2020;20(8):499–506.

18. Chapman NM, Chi H. Metabolic adaptation of lymphocytes in immunity and disease. Immunity. 2022;55(1):14–30.

19. Buck MD, O'Sullivan D, Klein Geltink RI, Curtis JD, Chang C-H, Sanin DE, et al. Mitochondrial dynamics controls T cell fate through metabolic programming. Cell. 2016;166(1):63–76.

20. Kurmi K, Liang D, van de Ven R, Georgiev P, Gassaway BM, Han S, et al. Metabolic modulation of mitochondrial mass during CD4+ T cell activation. Cell Chem Biol. 2023;30(9):1064.

21. Zakharov PN, Hu H, Wan X, Unanue ER. Single-cell RNA sequencing of murine islets shows high cellular complexity at all stages of autoimmune diabetes. J Exp Med. 2020. https://doi.org/10.1084/jem.20192362.

22. Julé AM, Hoyt KJ, Wei K, Gutierrez-Arcelus M, Taylor ML, Ng J, et al. Th1 polarization defines the synovial fluid T cell compartment in oligoarticular juvenile idiopathic arthritis. JCI Insight. 2021. https://doi.org/10.1172/jci.insight.149185.

23. Khan A, Roy P, Ley K. Breaking tolerance: the autoimmune aspect of atherosclerosis. Nat Rev Immunol. 2024;24(9):670–9.

24. Klehmet J, Hoffmann S, Walter G, Meisel C, Meisel A. Stroke induces specific alteration of T memory compartment controlling auto-reactive CNS antigen-specific T cell responses. J Neurol Sci. 2016;368:77–83.

25. Zhang Y, Wei L, Du Y, Xie Y, Wu W, Yuan Y. Association between programed cell Death-1 and CD4+ T cell alterations in different phases of ischemic stroke patients. Front Cell Neurosci. 2018;12:170.

26. Dotson AL, Chen Y, Zhu W, Libal N, Alkayed NJ, Offner H. Partial MHC constructs treat thromboembolic ischemic stroke characterized by early immune expansion. Transl Stroke Res. 2016;7(1):70–8.

27. Miró-Mur F, Urra X, Ruiz-Jaén F, Pedragosa J, Chamorro Á, Planas AM. Antigen-dependent T cell response to neural peptides after human ischemic stroke. Front Cell Neurosci. 2020;14:206.

28. Anthony S, Cabantan D, Monsour M, Borlongan CV. Neuroinflammation, stem cells, and stroke. Stroke. 2022;53(5):1460–72.

29. Li W, Shi L, Hu B, Hong Y, Zhang H, Li X, et al. Mesenchymal stem cell-based therapy for stroke: current understanding and challenges. Front Cell Neurosci. 2021;15:628940.

30. Feng Y-W, Wu C, Liang F-Y, Lin T, Li W-Q, Jing Y-H, et al. hUCMSCs mitigate LPS-induced trained immunity in ischemic stroke. Front Immunol. 2020;11:1746.

31. Huang Y, Wang J, Cai J, Qiu Y, Zheng H, Lai X, et al. Targeted homing of CCR2-overexpressing mesenchymal stromal cells to ischemic brain enhances post-stroke recovery partially through PRDX4-mediated blood-brain barrier preservation. Theranostics. 2018;8(21):5929–44.

32. Acosta SA, Tajiri N, Hoover J, Kaneko Y, Borlongan CV. Intravenous bone marrow stem cell grafts preferentially migrate to spleen and abrogate chronic inflammation in stroke. Stroke. 2015;46(9):2616–27.

33. Ercelen N, Karasu N, Kahyaoglu B, Cerezci O, Akduman RC, Ercelen D, et al. Clinical experience: Outcomes of mesenchymal stem cell transplantation in five stroke patients. Front Med. 2023;10:1051831.

34. Giacomini C, Granéli C, Hicks R, Dazzi F. The critical role of apoptosis in mesenchymal stromal cell therapeutics and implications in homeostasis and normal tissue repair. Cell Mol Immunol. 2023;20(6):570–82.

35. Pang SHM, D'Rozario J, Mendonca S, Bhuvan T, Payne NL, Zheng D, et al. Mesenchymal stromal cell apoptosis is required for their therapeutic function. Nat Commun. 2021;12(1):6495.

36. Yang Y, Ye G, Zhang Y-L, He H-W, Yu B-Q, Hong Y-M, et al. Transfer of mitochondria from mesenchymal stem cells derived from induced pluripotent stem cells attenuates hypoxia-ischemia-induced mitochondrial dysfunction in PC12 cells. Neural Regen Res. 2020;15(3):464–72.

37. Han D, Zheng X, Wang X, Jin T, Cui L, Chen Z. Mesenchymal stem/stromal cell-mediated mitochondrial transfer and the therapeutic potential in treatment of neurological diseases. Stem Cells Int. 2020;2020:8838046.

38. Akhter W, Nakhle J, Vaillant L, Garcin G, Le Saout C, Simon M, et al. Transfer of mesenchymal stem cell mitochondria to CD4+ T cells contributes to repress Th1 differentiation by downregulating T-bet expression. Stem Cell Res Ther. 2023;14(1):12.

39. Court AC, Le-Gatt A, Luz-Crawford P, Parra E, Aliaga-Tobar V, Bátiz LF, et al. Mitochondrial transfer from MSCs to T cells induces Treg differentiation and restricts inflammatory response. EMBO Rep. 2020;21(2):e48052.

40. Do J-S, Zwick D, Kenyon JD, Zhong F, Askew D, Huang AY, et al. Mesenchymal stromal cell mitochondrial transfer to human induced T-regulatory cells mediates FOXP3 stability. Sci Rep. 2021;11(1):10676.

41. Luz-Crawford P, Hernandez J, Djouad F, Luque-Campos N, Caicedo A, Carrère-Kremer S, et al. Mesenchymal stem cell repression of Th17 cells is triggered by mitochondrial transfer. Stem Cell Res Ther. 2019;10(1):232.

42. Piekarska K, Urban-Wójciuk Z, Kurkowiak M, Pelikant-Małecka I, Schumacher A, Sakowska J, et al. Mesenchymal stem cells transfer mitochondria to allogeneic Tregs in an HLA-dependent manner improving their immunosuppressive activity. Nat Commun. 2022;13(1):856.

43. Westendorp WF, Dames C, Nederkoorn PJ, Meisel A. Immunodepression, infections, and functional outcome in ischemic stroke. Stroke. 2022;53(5):1438–48.

44. Westendorp WF, Nederkoorn PJ, Vermeij J-D, Dijkgraaf MG, van de Beek D. Post-stroke infection: a systematic review and meta-analysis. BMC Neurol. 2011;11:110.

45. Hoffmann S, Malzahn U, Harms H, Koennecke H-C, Berger K, Kalic M, et al. Development of a clinical score (A2DS2) to predict pneumonia in acute ischemic stroke. Stroke. 2012;43(10):2617–23.

46. Jiao Y, Sun Y-T, Chen N-F, Zhou L-N, Guan X, Wang J-Y, et al. Human umbilical cord-derived mesenchymal stem cells promote repair of neonatal brain injury caused by hypoxia/ischemia in rats. Neural Regen Res. 2022;17(11):2518–25.

Chen *et al. Stem Cell Research & Therapy*   (2025) 16:134

Page 23 of 24

47. Dominici M, Le Blanc K, Mueller I, Slaper-Cortenbach I, Marini F, Krause D, et al. Minimal criteria for defining multipotent mesenchymal stromal cells: the international society for cellular therapy position statement. Cytotherapy. 2006;8(4):315–7.

48. Müller ML, Peglau L, Moon LDF, Groß S, Schulze J, Ruhnau J, et al. Neurotrophin-3 attenuates human peripheral blood T cell and monocyte activation status and cytokine production post stroke. Exp Neurol. 2022;347:113901.

49. Klimiec-Moskal E, Piechota M, Pera J, Weglarczyk K, Slowik A, Siedlar M, et al. The specific ex vivo released cytokine profile is associated with ischemic stroke outcome and improves its prediction. J Neuroinflamm. 2020;17(1):7.

50. Maecker HT, McCoy JP, Nussenblatt R. Standardizing immunophenotyping for the human immunology project. Nat Rev Immunol. 2012;12(3):191–200.

51. Brandi J, Wiethe C, Riehn M, Jacobs T. OMIP-93: A 41-color high parameter panel to characterize various co-inhibitory molecules and their ligands in the lymphoid and myeloid compartment in mice. Cytometry A. 2023;103(8):624–30.

52. Patananan AN, Sercel AJ, Wu T-H, Ahsan FM, Torres A, Kennedy SAL, et al. Pressure-driven mitochondrial transfer pipeline generates mammalian cells of desired genetic combinations and fates. Cell Rep. 2020;33(13):108562.

53. Chaparro-Cabanillas N, Arbaizar-Rovirosa M, Salas-Perdomo A, Gallizioli M, Planas AM, Justicia C. Transient middle cerebral artery occlusion model of stroke. J Vis Exp. 2023. https://doi.org/10.3791/65857.

54. Association AVM. AVMA Guidelines for the Euthanasia of Animals: 2020 Edition. Schaumburg, IL; 2020.

55. Longa EZ, Weinstein PR, Carlson S, Cummins R. Reversible middle cerebral artery occlusion without craniectomy in rats. Stroke. 1989;20(1):84–91.

56. Llovera G, Roth S, Plesnila N, Veltkamp R, Liesz A. Modeling stroke in mice: permanent coagulation of the distal middle cerebral artery. J Vis Exp. 2014;89:e51729.

57. Gagliani N, Amezcua Vesely MC, Iseppon A, Brockmann L, Xu H, Palm NW, et al. Th17 cells transdifferentiate into regulatory T cells during resolution of inflammation. Nature. 2015;523(7559):221–5.

58. Saravia J, Chapman NM, Chi H. Helper T cell differentiation. Cell Mol Immunol. 2019;16(7):634–43.

59. Zong Y, Deng K, Chong WP. Regulation of Treg cells by cytokine signaling and co-stimulatory molecules. Front Immunol. 2024;15:1387975.

60. Lei T-Y, Ye Y-Z, Zhu X-Q, Smerin D, Gu L-J, Xiong X-X, et al. The immune response of T cells and therapeutic targets related to regulating the levels of T helper cells after ischaemic stroke. J Neuroinflamm. 2021;18(1):25.

61. Faura J, Bustamante A, Miró-Mur F, Montaner J. Stroke-induced immunosuppression: implications for the prevention and prediction of post-stroke infections. J Neuroinflamm. 2021;18(1):127.

62. Klehmet J, Harms H, Richter M, Prass K, Volk HD, Dirnagl U, et al. Stroke-induced immunodepression and post-stroke infections: lessons from the preventive antibacterial therapy in stroke trial. Neuroscience. 2009;158(3):1184–93.

63. Restifo NP, Gattinoni L. Lineage relationship of effector and memory T cells. Curr Opin Immunol. 2013;25(5):556–63.

64. Simats A, Liesz A. Systemic inflammation after stroke: implications for post-stroke comorbidities. EMBO Mol Med. 2022;14(9):e16269.

65. Boshuizen MCS, Steinberg GK. Stem cell-based immunomodulation after stroke: effects on brain repair processes. Stroke. 2018;49(6):1563–70.

66. Cruz-Barrera M, Flórez-Zapata N, Lemus-Diaz N, Medina C, Galindo C-C, González-Acero L-X, et al. Integrated analysis of transcriptome and secretome from umbilical cord mesenchymal stromal cells reveal new mechanisms for the modulation of inflammation and immune activation. Front Immunol. 2020;11:575488.

67. Krishnan S, O'Boyle C, Smith CJ, Hulme S, Allan SM, Grainger JR, et al. A hyperacute immune map of ischaemic stroke patients reveals alterations to circulating innate and adaptive cells. Clin Exp Immunol. 2021;203(3):458–71.

68. Wang Z, He D, Zeng Y-Y, Zhu L, Yang C, Lu Y-J, et al. The spleen may be an important target of stem cell therapy for stroke. J Neuroinflamm. 2019;16(1):20.

69. Liu R, Song P, Gu X, Liang W, Sun W, Hua Q, et al. Comprehensive landscape of immune infiltration and aberrant pathway activation in ischemic stroke. Front Immunol. 2021;12:766724.

70. Lu J, Li H, Zhang G, Yang F, Zhang X, Ping A, et al. Age-related alterations in peripheral immune landscape with magnified impact on post-stroke brain. Research. 2023;6:0287.

71. Wang J, Gao Y, Yuan Y, Wang H, Wang Z, Zhang X. Th17 cells and IL-17A in ischemic stroke. Mol Neurobiol. 2023. https://doi.org/10.1007/s12035-023-03723-y.

72. Zhang Y, Liesz A, Li P. Coming to the rescue: regulatory T cells for promoting recovery after ischemic stroke. Stroke. 2021;52(12):e837–41.

73. Zhang H, Xia Y, Ye Q, Yu F, Zhu W, Li P, et al. In vivo expansion of regulatory T cells with IL-2/IL-2 antibody complex protects against transient ischemic stroke. J Neurosci. 2018;38(47):10168–79.

74. Ito M, Komai K, Mise-Omata S, Iizuka-Koga M, Noguchi Y, Kondo T, et al. Brain regulatory T cells suppress astrogliosis and potentiate neurological recovery. Nature. 2019;565(7738):246–50.

75. Benakis C, Simats A, Tritschler S, Heindl S, Besson-Girard S, Llovera G, et al. T cells modulate the microglial response to brain ischemia. Elife. 2022. https://doi.org/10.7554/eLife.82031.

76. Lee GR. The balance of Th17 versus treg cells in autoimmunity. Int J Mol Sci. 2018;19(3):730.

77. Chang D, Xing Q, Su Y, Zhao X, Xu W, Wang X, et al. The conserved noncoding sequences CNS6 and cns9 control cytokine-induced Rorc transcription during T Helper 17 cell differentiation. Immunity. 2020;53(3):614.

78. Dolati S, Ahmadi M, Khalili M, Taheraghdam AA, Siahmansouri H, Babaloo Z, et al. Peripheral Th17/Treg imbalance in elderly patients with ischemic stroke. Neurol Sci. 2018;39(4):647–54.

79. Papadopoulos A, Palaiopanos K, Björkbacka H, Peters A, de Lemos JA, Seshadri S, et al. Circulating interleukin-6 levels and incident ischemic stroke: a systematic review and meta-analysis of prospective studies. Neurology. 2022;98(10):e1002–12.

80. Kowalski RG, Ledreux A, Violette JE, Neumann RT, Ornelas D, Yu X, et al. Rapid activation of neuroinflammation in stroke: plasma and extracellular vesicles obtained on a mobile stroke unit. Stroke. 2023;54(3):e52–7.

81. Xia Y, Hu G, Chen Y, Yuan J, Zhang J, Wang S, et al. Embryonic stem cell derived small extracellular vesicles modulate regulatory T cells to protect against ischemic stroke. ACS Nano. 2021;15(4):7370–85.

82. Hu H, Li H, Li R, Liu P, Liu H. Re-establishing immune tolerance in multiple sclerosis: focusing on novel mechanisms of mesenchymal stem cell regulation of Th17/Treg balance. J Transl Med. 2024;22(1):663.

83. Zheng S, Huang K, Xia W, Shi J, Liu Q, Zhang X, et al. Mesenchymal stromal cells rapidly suppress TCR signaling-mediated cytokine transcription in activated t cells through the ICAM-1/CD43 interaction. Front Immunol. 2021;12:609544.

84. Wu B, Zhao TV, Jin K, Hu Z, Abdel MP, Warrington KJ, et al. Mitochondrial aspartate regulates TNF biogenesis and autoimmune tissue inflammation. Nat Immunol. 2021;22(12):1551–62.

85. Li Y, Wang Y, Yang W, Wu Z, Ma D, Sun J, et al. ROS-responsive exogenous functional mitochondria can rescue neural cells post-ischemic stroke. Front Cell Dev Biol. 2023;11:1207748.

86. Wang J, Zhao M, Wang M, Fu D, Kang L, Xu Y, et al. Human neural stem cell-derived artificial organelles to improve oxidative phosphorylation. Nat Commun. 2024;15(1):7855.

87. Peng H-Y, Lucavs J, Ballard D, Das JK, Kumar A, Wang L, et al. Metabolic reprogramming and reactive oxygen species in T cell immunity. Front Immunol. 2021;12:652687.

88. Man K, Kallies A. Synchronizing transcriptional control of T cell metabolism and function. Nat Rev Immunol. 2015;15(9):574–84.

89. Sun L, Fu J, Zhou Y. Metabolism controls the balance of Th17/T-regulatory cells. Front Immunol. 2017;8:1632.

90. Sena LA, Li S, Jairaman A, Prakriya M, Ezponda T, Hildeman DA, et al. Mitochondria are required for antigen-specific T cell activation through reactive oxygen species signaling. Immunity. 2013;38(2):225–36.

91. Yang M-Q, Zhang S-L, Sun L, Huang L-T, Yu J, Zhang J-H, et al. Targeting mitochondria: restoring the antitumor efficacy of exhausted T cells. Mol Cancer. 2024;23(1):260.

92. Scharping NE, Rivadeneira DB, Menk AV, Vignali PDA, Ford BR, Rittenhouse NL, et al. Mitochondrial stress induced by continuous stimulation under hypoxia rapidly drives T cell exhaustion. Nat Immunol. 2021;22(2):205–15.

93. Chávez MD, Tse HM. Targeting mitochondrial-derived reactive oxygen species in T cell-mediated autoimmune diseases. Front Immunol. 2021;12:703972.

Chen *et al. Stem Cell Research & Therapy*   *(2025) 16:134*

Page 24 of 24

94. Chen Y, Ye Y, Krauß P-L, Löwe P, Pfeiffenberger M, Damerau A, et al. Age-related increase of mitochondrial content in human memory CD4+ T cells contributes to ROS-mediated increased expression of proinflammatory cytokines. Front Immunol. 2022;13:911050.

95. Zhang Y, Li F, Chen C, Li Y, Xie W, Huang D, et al. RAGE-mediated T cell metabolic reprogramming shapes T cell inflammatory response after stroke. J Cereb Blood Flow Metab. 2022;42(6):952–65.

96. Wang X, Zhou Y, Tang D, Zhu Z, Li Y, Huang T, et al. ACC1 (acetyl coenzyme a carboxylase 1) is a potential immune modulatory target of cerebral ischemic stroke. Stroke. 2019;50(7):1869–78.

Publisher's Note